

Doctoral Dissertation

博士論文

Molecular mechanism underlying inter-organelle translocation of
piRNA precursor

(piRNA 生合成における前駆体のオルガネラ間輸送機構の解明)

A Dissertation Submitted for the Degree of Doctor of Philosophy
December 2019

令和元年 12 月博士（理学）申請

Department of Biological Sciences, Graduate School of Science,

The University of Tokyo

東京大学大学院理学系研究科生物科学専攻

Haruna Yamashiro

山城 はるな

Contents

Abstract.....	5
Abbreviations.....	8
Introduction.....	10
Transposon.....	11
RNA silencing	12
Characteristics of piRNAs.....	14
piRNA pathway in <i>Drosophila</i>	16
piRNA biogenesis	
in <i>Drosophila</i> ovarian somatic cells.....	17
Roles for Yb bodies	19
piRNA maturation on mitochondria.....	21
Gasz.....	21
Summary of this study	22
The aim of this study	24
Materials and methods	26
Cell culture	27
RNAi and plasmid transfection	27
Plasmid construction.....	28
Production of anti-Gasz monoclonal antibody	29
Western blotting.....	29
qRT-PCR	30

Northern blotting	31
Mitochondrial fractionation	31
Immunofluorescence analysis	32
Immunoprecipitation.....	33
Recombinant proteins	34
GST pull-down assay.....	34
Gel shift assay	35
Results	37
Armi aberrantly accumulates on mitochondria in the absence of Zuc but not upon Gasz loss	38
Gasz binds Armi–pre-piRISC complex on the outer membrane of mitochondria	41
ARs, SAM domain and mitochondrial localization of Gasz is required for piRNA biogenesis	42
pre-piRISC is formed in an Armi-dependent manner and translocated with Armi from Yb body to Gasz on mitochondria	43
Departure of Armi from Yb bodies depends on Piwi	44
Departure of Armi from Yb bodies requires piRNA precursor loading onto Piwi	46
The short form of Armi two isoforms lacks full-length's N- terminus which is important for piRNA biogenesis	47

Translocation of pre-piRISC from Yb bodies requires the RNA-binding activity and N-terminus of Armi	49
Discussion	52
Conclusion	57
Figures	59
Table	105
References	107
Acknowledgements	124

Abstract

Abstract

piRNAs assemble the piRNA-induced silencing complexes (piRISCs) with PIWI proteins to repress transposons for the integrity of germline genome. Without the piRNA function, transposons are derepressed, leading to failures in germline development and infertility.

piRNA biogenesis has been intensively studied using *Drosophila* ovarian somatic cells (OSCs). In OSCs, piRNA precursors are specifically bound with a Tudor domain-containing protein Yb, upon their nuclear export, which triggers the formation of cytoplasmic granules called Yb bodies. piRNA precursors are then processed within the bodies and the 5' end is bound with Piwi, one of *Drosophila* PIWI members, giving rise to Piwi-pre-piRISCs. Piwi-pre-piRISCs are in turn translocated to the surface of mitochondria, where an endonuclease Zucchini (Zuc) waits for them to produce mature Piwi-piRISCs from the precursor complexes. However, the regulatory mechanisms underlying the formation of Piwi-pre-piRISCs at Yb bodies and translocation to mitochondria remain elusive.

To address these questions, I studied the molecular mechanism using cultured OSCs and found that Armitage (Armi), a superfamily 1 (SF1) RNA helicase and a component of Yb bodies, is necessary for Piwi-pre-piRISC formation at Yb bodies and that Armi controls the exit of Piwi-pre-piRISCs from Yb bodies prior to

their translocation to mitochondria. Piwi-pre-piRISCs resisted leaving Yb bodies until Armi bound the pre-piRISCs through precursor RNAs. Loss of Armi N-terminus blocked the exit of pre-piRISCs from Yb bodies. I also found that a mitochondrial protein Gasz anchors Armi-Piwi-pre-piRISCs, facilitating Zuc-dependent Piwi-piRISC maturation. These findings suggest that Piwi-piRISC formation in OSCs is strictly regulated in a multilayered manner, from Piwi-pre-piRISC formation at Yb bodies, to the departure of pre-piRISC to mitochondria for its maturation. These elaborate mechanisms contribute to the quality control for piRNA biogenesis by avoiding the crosstalk among processing places.

Abbreviations

Abbreviations

Ago3	Argonaute3
Armi	Armitage
ARs	Ankyrin repeats
Aub	Aubergine
<i>C.elegans</i>	<i>Caenorhabditis elegans</i>
dsRNAs	double-stranded RNAs
<i>flam</i>	<i>flamenco</i>
KD	knockdown
LLPS	liquid–liquid phase separation
Mino	Minotaur
miRNAs	microRNAs
nts	nucleotides
OSCs	<i>Drosophila</i> ovarian somatic cells
piRNA	PIWI-interacting RNA
qRT-PCR	Quantitative Reverse Transcription Polymerase Chain Reaction
RNAi	RNA interference
RISC	RNA-induced silencing complex
SEM	standard error of the mean
SF1	superfamily 1
siRNAs	small interfering RNAs
ssRNAs	single-stranded RNAs
Shu	Shutdown
SoYb	Sister of Yb
S2	Schneider 2
Vret	Vreteno
Fs (1) Yb	female sterile (1) Yb
Zuc	Zucchini

Introduction

Introduction

Transposon

A wide range of organisms has allowed symbiosis between their own genomes and transposons over a long evolutionary period (Fedoroff 2012; Feschotte 2008). Transposons are non-self DNA elements, which can move around randomly (*i.e.*, transpose) in the genome (Slotkin and Martienssen 2007; Kazazian 2004). Transposons can be subdivided into DNA and RNA transposons, the latter of which are also known as retrotransposons. DNA transposons have the ability to remove themselves from, and insert themselves into, the genome, and they are considered “cut and paste” type transposons. RNA transposons are considered “copy and paste” transposons because RNA transcripts from these transposons are reverse-transcribed by their own enzymes and the resultant DNA fragments are inserted into the genome. The alteration of genome by transposon transposition is often advantageous evolutionally for the host living organisms, leading to their symbiosis. For example, transposons act as mutagens to enhance various abilities, allowing the organism to adapt and survive life-threatening environments. However, in parallel, their uncontrollable, selfish movement across the genome can cause DNA damage by insertion mutations. If this happens in the

germline cell, which is the only cell to be passed to next generation, gonadal development deteriorates, leading to infertility (Schupbach and Wieschaus 1991; Lin and Spradling 1997). Therefore, organisms have acquired an elaborative system for controlling transposons, particularly in the germline, namely the PIWI-interacting RNA (piRNA)-dependent transposon silencing mechanism.

RNA silencing

piRNA-dependent transposon silencing is one form of small RNA-mediated gene silencing, known as RNA silencing, which is a regulatory mechanism for controlling gene expression (Ghildiyal and Zamore 2009; Siomi and Siomi 2009; Wilson and Doudna 2013). In this pathway, small non-coding RNAs of 21–33 nucleotides (nts) guide Argonaute proteins to target gene transcripts by means of RNA-RNA base-pairings (Figure 1A). The Argonaute–small RNA complex is called the RNA-induced silencing complex (RISC) and its proper formation is required for gene regulation. RNA silencing occurs either transcriptionally or post-transcriptionally depending on subcellular localization of the RISC. Nuclear RISC represses target genes transcriptionally by remodeling chromatin via repressive histone modification and/or DNA methylation. Cytoplasmic RISC, on the other hand,

represses target genes post-transcriptionally, which is mainly dependent on target RNA cleavage via the endoribonuclease activity of Argonaute. This activity, known as Slicer activity, slices the target RNAs at a site facing the center of the guide RNA (Ghildiyal and Zamore 2009; Siomi and Siomi 2009). Some Argonaute members have no Slicer activity. In these cases, the proteins induce translational repression and/or mRNA decay by interacting with co-factors (Eulalio et al., 2008; Iwasaki et al., 2009).

Animals express multiple Argonaute family members, which are divided into two subclades, AGO and PIWI (Mochizuki et al., 2002). AGO subclade members (AGO proteins) are ubiquitously expressed and form RISCs with microRNAs (miRNAs) or small interfering RNAs (siRNAs), which are also ubiquitous. In contrast, PIWI subclade proteins (PIWI proteins) are expressed in germline only and form complexes with piRNAs called piRISCs.

miRNAs are derived from RNAs with imperfect hairpin structure, which are primarily transcribed as a longer precursor RNA and processed into mature miRNAs (Ha and Kim 2014; Davis-Dusenbery and Hata 2010)(Figure 1B). This processing requires Drosha and Dicer, both of which are RNase III endonucleases (Carthew and Sontheimer 2009; Ghildiyal and Zamore 2009; Kim et al., 2009). miRNAs mainly control the

expression of endogenous protein-coding genes by blocking translation or inducing mRNA instability.

siRNAs are processed from double-stranded (ds) RNAs by Dicer and repress the target gene expression. Ectopic expression of siRNAs is widely used for gene knockdown, which is called RNA interference (RNAi). RNAi was discovered in 1998 in a developmental study of the nematode *Caenorhabditis elegans* (*C.elegans*). RNAi in the study was artificially induced by injecting living *C. elegans* with dsRNAs, the guide RNAs of which were designed to be complementary to target genes (Fire et al., 1998). dsRNAs are processed into siRNAs, loaded onto AGO proteins to form RISCs, which then induce specific and efficient repression of complementary gene targets (Carthew and Sontheimer 2009; Ghildiyal and Zamore 2009; Kim et al., 2009) (Figure 1B). Technically, RNAi is inducible in any cell of any organism as long as the RNAi machinery is conserved.

Characteristics of piRNAs

piRNAs are germline-specific small noncoding RNAs which are bound to PIWI subclade proteins. PIWI proteins consist of four domains, N, PAZ, MID, and PIWI, and three linkers connecting the adjacent domains, L0, L1, and L2, similar to AGO proteins (Matsumoto et al., 2016). piRNAs normally range from 24–31 nt

in length, so they are slightly longer than siRNAs and miRNAs, which are normally 21–22 nt long. The 5'-end of piRNAs has a mono-phosphate, while the 3'-end is 2'-*O*-methylated (Saito et al., 2007; Brennecke et al., 2007; Gunawardane et al., 2007; Malone et al., 2009; Siomi et al., 2011; Ishizu et al., 2012; Iwasaki et al., 2015). A mono-phosphate at the 5'-end is also the characteristic of both miRNAs and siRNAs, indicating this is not unique to piRNAs. In *Drosophila*, 2'-*O*-methylation occurs in siRNAs but not in miRNAs (Horwich et al., 2007; Saito et al., 2007). The methyltransferase Hen1 catalyzes this modification in order to increase the stability of small RNAs *in vivo* (Horwich et al., 2007; Yu et al., 2005).

piRNAs originate from intergenic regions called piRNA clusters, which are rich in transposon sequences. These sequences correspond to various transposons but are fragmented and lack the ability to transpose in the genome. Therefore, piRNA clusters are considered transposon graveyards.

piRNAs are expressed in *dicer* mutants, indicating that piRNA processing is independent of Dicer (Vagin et al., 2006) (Figure 1B). In accordance with this, while siRNA/miRNA precursors are dsRNAs, piRNA precursors are single-stranded (ss) RNAs. piRNAs are specifically funneled onto PIWI proteins. Likewise, siRNAs and miRNAs are loaded onto AGO but not onto

PIWI proteins. PIWI- and AGO-mediated RNA silencing are independent of each other.

Genome-wide genetic screening has identified a large number of piRNA factors; the genes which are involved in piRNA pathway (Handler et al., 2013; Muerdter et al., 2013; Czech et al., 2013) Many factors are dedicated to piRNA biogenesis, while others play important roles in the effector (silencing) step of the pathway. When the functions of these factors are disturbed by mutations, transposon expression is derepressed in the germline, leading to infertility in various animals. In this way, piRNA-mediated transposon silencing is indispensable for prosperity of descendants.

piRNA pathway in *Drosophila*

The piRNA pathway is conserved among a wide range of animals including sponges, worms, mice, and humans (Figure 2A). *Drosophila melanogaster*, which is useful for genetic approach, has been widely used as the model for piRNA studies. *Drosophila* expresses three PIWI members, Piwi, Aubergine (Aub) and Argonaute3 (Ago3), which are expressed specifically in ovaries and testes (Gunawardane et al., 2007; Cox et al., 1998; Harris et al., 2001). Loss of any one of the three PIWI members cause derepression of transposons in *Drosophila* (Li et al., 2009; Vagin

et al., 2006) (Figure 2B), suggesting no functional redundancy in the PIWI proteins. In germ cells, Aub and Ago3 are localized in the cytoplasm and they repress transposons by cleaving target RNA transcripts using their Slicer activity (Brennecke et al., 2007; Gunawardane et al., 2007). Slicer-dependent cleavage occurs on target RNAs between the 10-11 nts relative to piRNAs, which is also known as ping-pong pathway (Brennecke et al., 2007; Gunawardane et al., 2007; Li et al., 2009).

Aub and Ago3 are not expressed in gonadal somatic cells (Figure 3). In contrast, Piwi is expressed in both germ and gonadal somatic cells, where Piwi is localized in the nucleus to silence transposons epigenetically by inducing heterochromatinization through histone H3K9 trimethylation (H3K9me3) at genomic loci where active transposons are present (Cox et al., 2000; Huang et al., 2013; Klenov et al., 2011; Sienski et al., 2012; Thomas et al., 2013; Wang et al., 2011)(Figure 3).

piRNA biogenesis in *Drosophila* ovarian somatic cells

A cultured cell line derived from *Drosophila* ovarian somatic cells (OSCs) was established in 2009 (Saito et al., 2009). OSCs have been widely used as a powerful tool for the study of piRNA pathway because the materials are suitable for biochemical approaches. Another advantage for using OSCs is to investigate

the mechanism underlying biogenesis of Piwi-bound piRNAs, excluding the effect of other PIWI members.

In OSCs, piRNA biogenesis starts with transcription of precursors from piRNA clusters (Figure 4). A representative cluster in *Drosophila* ovarian somatic cells is *flamenco* (*flam*). The *flam* locus is rich in transposon remnants, whose directions at the locus are mostly opposite to the direction of *flam* transcription (Brennecke et al., 2007; Prud'homme et al., 1995). Therefore, by their nature, *flam*-derived piRNAs are created to act as antisense oligonucleotides to silence their parental transposons (Brennecke et al., 2007; Zanni et al., 2013; Goriaux et al., 2014). The processing of piRNA precursors in the nucleus is similar to that of mRNA precursors, *i.e.*, 5' capping, splicing, and poly(A) addition, before being exported to the cytoplasm to produce mature piRNAs (Goriaux et al., 2014).

Eight proteins have so far been designated as piRNA biogenesis factors in OSCs: Female sterile (1) Yb (Yb), Armitage (Armi), Sister of Yb (SoYb), Vreteno (Vret), Shutdown (Shu), Zucchini (Zuc), Minotaur (Mino) and Gasz (Figure 4). These factors can be classified into two groups by their apparent cellular localization in OSCs. Yb, Armi, SoYb, Vret, and Shu are detected at the perinuclear non-membranous organelles called Yb bodies (Handler et al., 2011; Olivieri et al., 2010; Olivieri et al., 2012; Saito et al., 2010; Szakmary et al., 2009), whose assembly is

required for transposon-repressing piRNA production (Hirakata et al., 2019). In contrast, Zuc, Mino and Gasz are localized at the outer membrane of mitochondria via their own transmembrane targeting signals (TMs) (Handler et al., 2013; Ipsaro et al., 2012; Mohn et al., 2015; Nishimasu et al., 2012; Vagin et al., 2013). However, the rest of the protein bodies projects towards the cytosol, allowing them to act in piRNA biogenesis together with other cytosolic factors.

After the assembly of piRISCs, they translocate to nucleus. piRNA loading of Piwi triggers conformational change of Piwi and enable piRISC to interact with nuclear import factor, Importin α (Yashiro et al., 2018). This piRNA-loading-dependent regulatory system is required because nuclear Piwi without piRNAs lack a target, which might cause dominant negative effects in the pathway.

Roles for Yb bodies

Yb is a Tudor domain-containing protein (Szakmary et al., 2009), which self-associates and binds to the *flam* RNA transcripts (*i.e.*, transposon-repressing piRNA precursors) through the *cis*-elements within the precursors (Hirakata et al., 2019; Homolka et al., 2015; Ishizu et al., 2015; Murota et al., 2014). The *cis*-elements were identified as the sequences that drive piRNA biogenesis but

those clear characteristics remain to be defined. The multivalent association between Yb and *flam* RNAs induces liquid-liquid phase separation (LLPS), leading to the assembly of Yb bodies (Hirakata et al., 2019). piRNA precursors are then processed within the bodies and the 5' end is bound with Piwi, giving rise to pre-piRISCs. The precursors in this context are pre-bound with Piwi through their 5' end to form Piwi-pre-piRISCs. Hereinafter, in this thesis, I refer to Piwi-pre-piRISCs as pre-piRISCs because other types of pre-piRISCs such as Aub-pre piRISCs are not expressed in OSCs.

Armi is a superfamily 1 (SF1) RNA helicase exhibiting ATP-dependent, 5'-to-3' directional RNA-unwinding activity (Ishizu et al., 2019; Pandey et al., 2017), subsequently joins Yb bodies by associating with Yb, in order to bind specifically to *flam* RNAs (Ishizu et al., 2019; Ge et al., 2019). In the absence of Yb, Yb bodies disappeared and Armi shows dispersed cytoplasmic location (Olivieri et al., 2010; Saito et al., 2010). Upon Yb depletion, Armi binds cellular RNAs promiscuously and produces piRNAs from the bound RNAs (Ishizu et al., 2019). This means that piRNA production in OSCs does not always require Yb (and Yb body formation). However, the expression levels of piRNAs become low and those piRNAs are mostly non-transposon-targeting. Thus, Yb bodies are considered to be important for recognition and

accumulation of correct piRNA precursors in order to ensure effective repression of transposon expression.

piRNA maturation on mitochondria

After the processing at Yb bodies, piRNA precursors are matured on mitochondria. Zuc is an endoribonuclease responsible for excising mature piRNAs successively from the 5' end of the precursors, giving rise to phased piRNAs (Han et al., 2015; Mohn et al., Homolka et al., 2015). Pre-piRISC are cleaved by Zuc to produce the 3' end of mature piRNAs (Han et al., 2015; Mohn et al., Homolka et al., 2015). *In vitro* cleavage assay showed that Zuc has no ability to recognize the sequence of substrates (Nishimasu et al., 2012; Nishida et al., 2018). Based on these results, how piRNA precursors are discriminated from other cellular RNAs and funneled into piRNA maturation machinery on mitochondria remains elusive.

Gasz

Gasz (Figure 5A) was identified as a piRNA factor in previous research of *Drosophila* genetic screening (Handler et al., 2013; Czech et al., 2013). The phenotype of Gasz knockdown (KD) shows strong derepression of transposons and infertility (Figure 5B). It

is also reported that Gasz is involved in piRNA pathway in other animals including mice (Ma et al., 2009), suggesting the importance of its function. Gasz contains six Ankyrin repeats (ARs), a SAM domain and a transmembrane predicted region, by which Gasz is localized on mitochondria (Handler et al., 2013) (Figure 5C). ARs are known to function in protein-protein interactions and a SAM domain is known to have RNA binding or dimer formation activity (Figure 5A) (Kim and Bowie 2003; Li et al., 2006; Mosavi et al., 2004). According to this domain structure, Gasz is predicted to have the role as the scaffold on mitochondria for Zuc-dependent piRNA maturation.

Summary of this study

The purpose of this study is to elucidate the molecular mechanism underlying the inter-organelle translocation of piRNA precursor in piRISC processing. To this end, I provide evidence to claim that:

1. Armi is required for pre-piRISC assembly at Yb bodies.
2. The 5'-binding pocket in the MID domain of Piwi, but not the 3'-binding pocket in the PAZ domain, is essential for Piwi-piRNA precursor interaction.

3. Armi recognize pre-piRISC assembly at Yb bodies and triggers its exit from Yb bodies before the complex heads to mitochondria.
4. pre-piRISC resists leaving Yb bodies until Armi binds pre-piRISC through precursor RNA.
5. Lack of 34 N-terminal residues in Armi also abrogates pre-piRISC leaving Yb bodies.
6. The Armi–pre-piRISC complex anchored through Gasz on the surface of mitochondria indeed contains *flam*-piRNA precursor, whose processing by Zuc depends on also Gasz.
7. ARs and SAM domain of Gasz are indispensable for piRNA biogenesis.

In summary, this study clarified how piRISC processing is under control, in a multilayered manner, from pre-piRISC and Armi–pre-piRISC complex formation at Yb bodies, the departure of the complex from Yb bodies, and to inter-organelle translocation of the complex to reach mitochondria. In this processing, the regulation of protein–protein or protein–RNA interaction and the function of Armi N-terminus are required. Without any of these regulations, transposon-repressing piRISC is not formed, leading to transposon de-repression. Thus, all processes, that I found in this study, governs quality control for piRNA biogenesis and the integrity of germline genome.

The aim of this study

The aim of this study

In order to produce piRISCs, which can recognize correct targets for silencing, it is very important for piRNA precursors to be discriminated from other cellular RNAs and directed to piRNA biogenesis pathway via Yb bodies and the surface of mitochondria. However, the regulatory mechanism(s) underlying the formation of pre-piRISCs at Yb bodies and the translocation from Yb bodies to mitochondria, the site for piRISC maturation, remains elusive. In this study, to shed light on the piRISC processing pathway between two organelles, I firstly tried to clarify the function of Gasz. To this end, I investigated the phenotype of Gasz depletion in OSCs and the interaction between Gasz and other piRNA biogenesis factors. I also conducted the mutant analysis of Gasz. Furthermore, in order to understand the step-by-step regulation of pre-piRISC processing, I conducted KD experiments of various combination and various mutant experiments. The main goal of my study is to understand the molecular mechanism underlying the inter-organelle translocation of pre-piRISC between Yb bodies and mitochondria.

Materials and methods

Materials and methods

Cell culture

OSCs were cultured at 26°C in Shields and Sang M3 medium (USBiological) supplemented with 10% fetal bovine serum (Funakoshi), 0.6 mg/mL glutathione, 10 mU/mL insulin, and 10% fly extract. The fly extract was prepared by heat-inactivating the supernatant of homogenized flies (0.2 g/mL adult Oregon R flies in Shields and Sang M3 medium supplemented with 10% FBS) at 60°C for 5 min. S2 cells were cultured at 26°C in Schneider's Drosophila medium (Gibco) supplemented with 10% fetal bovine serum (Equitech-Bio), and 1 × penicillin–streptomycin–glutamine (Gibco).

RNAi and plasmid transfection

For RNAi of OSCs, 5.0×10^6 cells were suspended in 20 μ L of Solution SF of the Cell Line Nucleofector Kit SF (Lonza Bioscience) with 200–400 pmol siRNAs. Electroporation was performed by the DG-150 program of a Nucleofector 96-well Shuttle device (Lonza Bioscience). The sequences of the siRNAs used in this study are shown in Table 1. For the control of RNAi, I use siEGFP. For plasmid transfection or plasmid and siRNA co-

transfection, 1.5×10^7 cells were suspended in 100 μ L of transfection buffer [180 mM sodium phosphate buffer for Church and Gilbert hybridization (pH 7.2), 5 mM KCl, 15 mM MgCl₂, 50 mM D-mannitol; modified from (Nye et al., 2014)] with 2–10 μ g of plasmids and 600–1200 pmol siRNAs. Electroporation was performed by the N-020 program of a Nucleofector 2b device (Lonza Bioscience). In the RNAi experiments, cells were transfected with siRNAs twice every 48 h and harvested 48 h later. In the rescue assays, endogenous gene was knocked down by RNAi 48 h before transfection of both plasmids and siRNA, and cells were harvested 48 h later.

Plasmid construction

To construct Myc-Gasz⁻, Flag-Gasz⁻, and GST-Gasz-expressing plasmids, a full-length gasz cDNA was amplified from OSC mRNAs by RT-PCR and cloned into pAcM, pAcF, and pGEX vectors, respectively. Expression vectors of Myc-Gasz mutants (Δ AR1, Δ AR2, Δ SAM, Δ TM) were generated by inverse PCR using Myc-Gasz WT vector. Expression vector of Armi-Flag WT was produced by inverse PCR and infusion using the RNAi-resistant Flag-Armi WT vector (Ishizu et al., 2019) as a template. Expression vectors of Armi-Flag mutants (N756A and Δ N34) were generated by inverse PCR using Armi-Flag WT vector. Armi-Flag

means that a Flag peptide was added to the C-terminal end of Armii. Flag-Armii means that a Flag peptide was added to the N-terminal end of Armii. Expression vectors of Flag-tagged Piwi mutants (PAZmt and MIDmt) were generated by inverse PCR and infusion, using the RNAi-resistant Myc-Piwi PAZmt vector (Saito et al., 2010) and the RNAi-resistant Flag-Piwi WT vector (Yashiro et al., 2018) as templates, respectively. To construct Luc-Flag-expressing vector, a full-length luciferase cDNA was amplified from firefly mRNAs by RT-PCR and cloned into pAcF vector. The primers used are summarized in Table 1.

Production of anti-Gasz monoclonal antibody

Recombinant proteins of full-length Gasz fused to glutathione S-transferase (GST) (GST-Gasz) were expressed in and purified from *E. coli*, and then injected into mice for immunization. The production and selection of hybridomas that produced anti-Gasz monoclonal antibodies were performed as described previously (Nishida et al., 2015).

Western blotting

Western blotting was performed in principle as described previously (Miyoshi et al., 2005). The primary antibodies used in

this study were anti-Armi monoclonal antibody (2F8A9, 1:1,000 dilution; Saito et al., 2010 , 2D6E11, supernatant of hybridoma cells), anti-Piwi monoclonal antibody (3G11, 1:1,000 dilution ;Saito et al., 2006), anti-Yb monoclonal antibody (8H12D12, 1:1,000 dilution ;Murota et al., 2014), anti-Gasz monoclonal antibody (1:1,000 dilution, this study), anti-Vret monoclonal antibody (1:1,000 dilution; Hirakata et al., 2019), anti-SoYb monoclonal antibody (1:1,000 dilution, Hirakata et al., 2019), anti- β -Tubulin monoclonal antibody (1:1,000 dilution, E7, Developmental Studies Hybridoma Bank), anti-HSP60 monoclonal antibody (1:2,000 dilution, LK1, StressMarq Biosciences), anti-Myc monoclonal antibody (9E10, 1:1,000 dilution, Fujifilm Wako Pure Chemical), and anti-Flag monoclonal antibody (FLA-1, 1:10,000 dilution, Medical & Biological Laboratories). Peroxidase-conjugated anti-mouse IgG antibodies (1:5,000 dilution, Cappel) were used as secondary antibodies. The signal intensity of bands was quantified by Image J (National Institutes of Health). All the experiments were performed at least three times to draw each conclusion.

qRT-PCR

Total RNAs were isolated from OSCs using ISOGEN II (NIPPON GENE), followed by DNase treatment. 1 μ g of total RNA was

reverse-transcribed using a ReverTra Ace qPCR RT Master Mix (TOYOBO), and the resulting cDNAs were amplified with PowerUp SYBR Green Master Mix (Thermo Fisher Scientific) using StepOnePlus (Thermo Fisher Scientific). The sequences of the primers used in this study are shown in Table 1. Cells were prepared by three independent transfection experiments.

Northern blotting

Northern blotting was carried out as described previously (Saito et al., 2005). Total RNAs were isolated from OSCs using ISOGEN II (Fujifilm Wako Pure Chemical). RNAs in immunoprecipitated complex were eluted from beads with phenol–chloroform and precipitated with ethanol. The oligodeoxynucleotides used as probes are shown in Table 1. All the experiments were performed at least three times to draw each conclusion.

Mitochondrial fractionation

Mitochondrial fractionation of OSC lysates was performed as previously reported (Wieckowski et al., 2009) with some modifications. Briefly, 1.2×10^8 cells were suspended with 500 μ L of buffer for first resuspension [30 mM Tris-HCl (pH 7.3), 225 mM D-mannitol, 75 mM sucrose, 0.05 mM EGTA] and ruptured by

passing 30 times through a 30-gauge needle attached to a 1-mL syringe. The lysates were centrifuged at 600g for 5 min and the pellets of nucleus and cell debris were discarded. This step was repeated twice. The lysates were centrifuged at 7,000g for 10 min and the supernatants were collected as the cytoplasmic fraction. The pellets were collected and resuspended with 500 μ L of buffer for the second resuspension [30 mM Tris-HCl (pH 7.3), 225 mM D-mannitol, 75 mM sucrose]. This step was repeated three times at 7,000g for 10 min and two times at 10,000g for 10 min. The final pellets were collected as the mitochondrial fraction. Proteins in each fraction were detected by western blotting. For “mito” blot, we used mitochondria isolated from 5 volumes of total lysates used in the “total” blot.

Immunofluorescence analysis

Immunofluorescence analysis was essentially performed as described previously (Saito et al., 2010). Primary antibodies used in this study were anti-Yb monoclonal antibody (8H12D12, 1:200 dilution, 1G2H3, 1:100 dilution; Murota et al., 2014), anti-Armi monoclonal antibody (2F8A9, 1:200 dilution), anti-Piwi monoclonal antibody (4D2, 1:200 dilution; Saito et al., 2006), and anti-Flag monoclonal antibody (FLA-1, 1:5,000 dilution). The secondary antibodies used in this study were Alexa 488-

conjugated anti-mouse IgG1, Alexa 488-conjugated anti-mouse IgG2a, Alexa 488-conjugated anti-mouse IgG2b, Alexa 555-conjugated anti-mouse IgG1, Alexa 555-conjugated anti-mouse IgG2a, Alexa 555-conjugated anti-mouse IgG2b, and Alexa 633-conjugated anti-mouse IgG2a (all from Thermo Fisher Scientific). All secondary antibodies were used at 1:1,000 dilution. Before fixation, the cells were incubated with MitoTracker Orange CMXRos (1:2,000 dilution, Invitrogen) for 15 min at 26°C. The cells were mounted with VECTASHIELD Mounting Medium with DAPI (Vector Laboratories), followed by observation using an LSM 710 laser scanning confocal microscope (Carl Zeiss). More than 15 cells were analyzed, and representative images are shown.

Immunoprecipitation

Immunoprecipitation was primarily performed as described previously; Saito et al., 2010. Cells were suspended with binding buffer [30 mM HEPES-KOH (pH 7.3), 150 mM KOAc, 5 mM Mg(OAc)₂, 5 mM DTT, 1.0% Triton X-100, 2 µg/mL leupeptin, 2 µg/mL pepstatin A, 0.5% aprotinin] and ruptured by passing 10 times through a 30-gauge needle attached to a 1-mL syringe. Cell lysate was incubated with antibodies bound to Dynabeads Protein G (Thermo Fisher Scientific) at 4°C for 1 h. The beads were washed five times with binding buffer. Eluted proteins were separated on

SDS polyacrylamide gels and detected by western blotting (see above).

Recombinant proteins

Purification of GST-fused proteins was mainly performed as described previously (Nishida et al., 2015). Briefly, GST-fused proteins were expressed in *E. coli* and were resuspended with lysis buffer [20 mM Tris-HCl (pH 7.5), 500 mM NaCl, 1.0% Triton X-100, 1 × cOmplete™ ULTRA Tablets, EDTA-free, glass vials Protease Inhibitor Cocktail (Sigma), 1 mM DTT] and lysed by sonication (BRANSON Digital Sonifier 250) at 20% amplitude for 3 min total sonication (180 cycles of 0.2 s sonication followed by 0.8 s rest). The supernatants after centrifugation were bound to Glutathione Sepharose 4B (GE Healthcare) and washed five times with lysis buffer. The proteins were eluted with elution buffer [20 mM Tris-HCl (pH 9.0), 150 mM NaCl, 1.0% Triton X-100, 1 mM DTT, 10 mM glutathione, 10% glycerol]. The eluted proteins were dialyzed in dialysis buffer [20 mM Tris-HCl (pH 7.5), 150 mM NaCl, 1 mM DTT, 10% glycerol]. Recombinant Armi protein was purified as previously described (Ishizu et al., 2019).

GST pull-down assay

GST pull-down assay was performed as previously reported (Nguyen et al., 2006) with some modifications. Briefly, GST-fused proteins were bound to Glutathione Sepharose 4B in binding buffer [30 mM HEPES-KOH (pH 7.3), 150 mM KOAc, 5 mM Mg(OAc)₂, 5 mM DTT, 1.0% Triton X-100, 2 µg/mL leupeptin, 2 µg/mL pepstatin A, 0.5% aprotinin] by rotation at 4°C for 1 h. Beads were washed with high-salt wash buffer [30 mM HEPES-KOH (pH 7.3), 500 mM NaCl, 150 mM KOAc, 5 mM Mg(OAc)₂, 5 mM DTT, 1.0% Triton X-100, 2 µg/mL leupeptin, 2 µg/mL pepstatin A, 0.5% aprotinin] twice and with binding buffer twice. The beads and Armi-Flag proteins were rotated at 4°C for 1 h. Beads were washed with wash buffer four times. Proteins were eluted with SDS sample buffer, separated on SDS polyacrylamide gels, and detected by western blotting or CBB staining.

Gel shift assay

Gel shift assays were carried out as previously described (Ishizu et al., 2019). For this assay, 16-nt ssRNA was radioactively 5'-end-labeled with [γ -³²P]ATP using T4 PNK. Reaction mixtures of 10 µl containing 50 mM Tris-HCl (pH 7.5), 50 mM KOAc, 2 mM Mg(OAc)₂, 1 mM DTT, 1 U/µl RNasin, 1 nM ssRNA, and purified proteins were incubated for 15 min at 25°C. After incubation, 2 µl of sample buffer (0.1% bromophenol blue, 0.1% xylene cyanol, and

50% glycerol) was added. The RNA–protein complexes were separated in 5% nondenaturing Tris–glycine gel. The gels were dried and the RNA–protein complexes were visualized by phosphorimaging.

Results

Results

Armi aberrantly accumulates on mitochondria in the absence of Zuc but not upon Gasz loss

I first set out to confirm the importance of Gasz for piRNA biogenesis in OSCs. To understand the function of Gasz, I produced anti-Gasz monoclonal antibody. Gasz was downregulated by RNAi and its expression level was confirmed by western blotting (Figure 6). qRT-PCR and Northern blotting were performed to examine transposon expression and piRNA accumulation, respectively. Upon Gasz depletion, the expression level of transposon was derepressed severely (Figure 7A) and mature *idefix*-piRNA, which is arising from the *flam* locus, almost disappeared. These findings corroborated the importance of Gasz in piRNA biogenesis. In parallel with this, Zuc was depleted as a positive control (Nishimasu et al., 2012; Murota et al., 2014). Without Gasz, the long piRNA precursors strongly accumulated, as was the case upon Zuc depletion (Figure 7B). This result suggests that Gasz is involved in Zuc-dependent piRNA maturation from piRNA precursors.

As described above (**Introduction: Gasz**), Gasz is predicted to have the role as the scaffold on mitochondria. In order to explore the candidate factors which transport piRNA precursors from Yb

body (Figure 4), I isolated mitochondria from OSC cytoplasmic lysate and examined the levels of endogenous Gasz, Piwi, and four Yb-body components (*i.e.*, Armi, SoYb, Yb, and Vret) in the fraction and also in the cytoplasmic lysate after mitochondrial isolation. Gasz was detected in the mitochondrial fraction, as was the mitochondrial marker protein HSP60 (Figure 8). Piwi and Armi were also present in the mitochondrial fraction, although their levels were much lower than those in the mitochondrion-depleted cytoplasmic fraction. SoYb, Yb, and Vret were nearly exclusively cytoplasmic. This result supports the idea that Armi is involved in the translocation of pre-piRISC from Yb body to mitochondria.

I then compared the levels of mitochondrial Piwi and Armi in the presence and absence of Zuc. The band intensity of mitochondrial Piwi was increased upon Zuc depletion (~1.7-fold) (Figure 9A). Strikingly, the accumulation of Armi in the mitochondrial fraction was higher upon Zuc depletion (~4.2-fold). The data from immunofluorescence analyses agreed with this: the Armi signal was strongly overlapped with the mitochondrial signal upon Zuc depletion (Figure 9B), while Armi in normal OSCs was detected at Yb bodies, as previously reported (Olivieri et al., 2010; Saito et al., 2010). Yb bodies were present even in Zuc-lacking OSCs (Figure 10). These results suggest that Armi exporting from Yb body is stuck on mitochondria when Zuc-dependent piRNA processing is inhibited (Figure 9C). Piwi was

mostly mislocalized to the cytoplasm and Yb body, due to loss of piRNA loading while Piwi is mainly localized in nucleus when Piwi forms piRISC (Figure 10; Yashiro et al., 2018). The mitochondrial localization of Piwi was unclear (Figure 10). This might be attributable to the reduced level of Piwi due to the loss of piRNA loading (Figure 9A). Zuc knockdown caused slightly mitochondrial clustering in OSCs (Figure 9B), as has been reported previously (Olivieri et al., 2012), although at present the effect of this phenomenon on piRNA biogenesis remains unclear.

Curiously, additional knockdown of Gasz in Zuc-lacking OSCs reduced the amount of Armi in mitochondrial fraction (~0.34-fold) (Figure 11A). The findings from immunofluorescence analysis agreed with this observation and showed that Gasz depletion restored the Yb-body localization of Armi (Figure 11B). Single depletion of Gasz had little impact on the Yb-body localization of Armi (Figure 12). These results suggest that, without Gasz, regardless of the presence or absence of Zuc, Armi exporting from Yb body no longer remains on the mitochondrial surface (Figure 11C). Changes in Piwi abundance and localization were not so drastic between before and after Gasz knockdown in Zuc-lacking OSCs (~0.68-fold) (Figure 11A) and showed largely cytosolic and Yb-body localization. (Figure 10). The dynamics of Piwi between Yb body and mitochondria is hard to observe in terms of localization analysis. Previous studies showed that Gasz

loss perturbs mitochondrial morphology in OSCs (Handler et al., 2013), which was also observed but to a lesser extent in this study (Figure 12).

By integrating all circumstantial evidence that has so far been clarified, Armi is translocated from Yb body to mitochondria in a Gasz-dependent manner. Upon piRISC formation by Zuc on the mitochondrial surface, Armi goes away from mitochondria to cytosol, while Piwi–piRISC is imported into the nucleus. However, the physical relationship among Armi, Piwi and Gasz remains unclear.

Gasz binds Armi–pre-piRISC complex on the outer membrane of mitochondria

To examine whether Armi and Piwi in the mitochondrial fraction are in a bound form with Gasz, we prepared the mitochondrial fraction, immunopurified the Gasz complex from the mitochondrial lysate, and conducted western blotting. Both Armi and Piwi were detected in the immunopurified material (Figure 13), indicating that Armi, Piwi, and Gasz form a trimeric complex on the outer membrane of mitochondria. The abundance of Armi and Piwi in the Gasz complex was increased upon Zuc depletion (Figure 14) in accordance with the results shown in Figure 9. I then performed northern blotting using the *idefix*-piRNA probe as

in Figure 7B. *flam*-piRNA precursors, albeit at very low levels, were detected in the Gasz complex in normal OSCs (Figure 14). The precursor signal was greatly increased upon Zuc depletion as were Armi and Piwi signals. These results provide evidence that Piwi and Armi are bound with mitochondrial Gasz in a complex that includes *flam*-piRNA precursors.

ARs, SAM domain and mitochondrial localization of Gasz is required for piRNA biogenesis

In order to understand the role of Gasz in detail, I analyzed the function of its protein domains. I produced four Gasz deletion mutants; Δ AR1, Δ AR1-2, Δ SAM and Δ TM by deleting the AR1 only or both AR1 and AR2 from the N-terminal end, SAM domain from the middle of the protein, and transmembrane from C-terminal end, respectively (Figure 15A). After endogenous Gasz was repressed by RNAi, these mutants were expressed by transfection (Figure 15B). Although Δ AR1, Δ AR2 and Δ SAM mutants were localized on mitochondria as well as WT (Figure 16), these mutants cannot rescue piRNA loss induced by Gasz depletion (Figure 17). These results suggest that ARs and SAM domains are indispensable for piRNA biogenesis. Δ TM mutant was dispersed to cytosol (Figure 16) and disturbed piRNA

biogenesis (Figure 17B), indicating that mitochondrial localization of Gasz is important for effective piRNA biogenesis.

Yb bodies are often observed to be near mitochondria (Murota et al., 2014). Does Gasz interact directly with Armi and Piwi which are localized at Yb body (Figure 18A)? Or does Gasz receive Armi and Piwi which are apart from Yb body (Figure 18B)? In order to answer the question, I examined whether Δ TM mutant is accumulated to Yb body or not. If the former model is correct, Δ TM mutant is supposed to accumulate at Yb body because Δ TM mutant is not anchored to mitochondria. As a result, Δ TM mutant did not accumulate with Armi which is at Yb body, supporting the latter model (Figure 18C). Previous study showed that Zuc and Gasz are localized on all over mitochondria while Yb bodies are a few in a cell (Handler et al., 2013). These results suggest that the Armi-Piwi complexes have the ability to be delivered from Yb body to all over the mitochondria in a cell.

pre-piRISC is formed in an Armi-dependent manner and translocated with Armi from Yb body to Gasz on mitochondria

The interaction between Armi and Piwi remained stable even after Gasz depletion (Figure 19A), suggesting that the Armi-pre-piRISC complex is formed prior to binding Gasz. Previous study proposed that Piwi was barely localized to Yb bodies without Armi

regardless of the presence of Yb bodies in OSCs (Saito et al., 2010). In this study, I observed that Piwi was no longer associated with piRNA precursors upon loss of Armi (Figure 19B). Thus, Piwi requires Armi to be loaded with the precursors at Yb bodies. These findings revealed that pre-piRISC is formed at Yb bodies in an Armi-dependent manner.

Summarizing my data so far, pre-piRISC is formed in an Armi-dependent manner at Yb body and translocated together to Gasz platform on mitochondria (Figure 20). I clarified not only the function of Gasz in piRNA biogenesis but also the intracellular dynamics of pre-piRISC. However, the regulatory mechanism underlying the inter-organelle translocation of pre-piRISC remains to be elucidated. I therefore aim to address the question by KD and mutant experiments.

Departure of Armi from Yb bodies depends on Piwi

I depleted Piwi in Zuc-depleted OSCs and performed immunofluorescence. Strikingly, the aberrant mitochondrial accumulation of Armi induced by Zuc loss was completely released upon additional Piwi depletion and Armi localization to Yb bodies was fully restored (Figures 21A-C). Western blotting confirmed that this was not due to unexpected reduction in the level of Armi (Figure 21D). The immunofluorescence data also showed that Yb-

body localization of Armi occurs in a Piwi-independent manner (Figures 21B-C). Previous study proposed that Piwi's Yb-body localization depends on Armi (Saito et al., 2010). The hierarchy of Piwi and Armi in Yb-body localization was clarified.

I also found that under these conditions, Armi no longer stably associated with Gasz (Figure 22). I postulated two scenarios to explain this: Without Piwi, (1) Armi resists leaving Yb bodies and thus is stuck there, or (2) Armi leaves Yb bodies and moves to mitochondria but cannot remain there, possibly because of loss of the ability to attach to Gasz (Figure 23).

In order to answer the question, I performed *in vitro* pull-down assay and demonstrate that recombinant Armi [purified from S2 cells under harsh conditions, preventing co-purification of other proteins (Ishizu et al., 2019)] bound with recombinant Gasz lacking the C-terminal TM region (Δ C113), which was bacterially purified, without any other factors (Figure 24); this supports their ability to directly interact with each other. My study also demonstrate that Gasz and Armi interact with each other in S2 cells (Figure 25) where Yb and Piwi are not expressed (Sumiyoshi et al., 2016). These results show that Armi cannot translocate from Yb body to mitochondria without Piwi although Armi can bind directly with Gasz. These findings more strongly support the first scenario that Armi resists leaving Yb bodies unless Piwi localizes to Yb bodies to become pre-piRISC there.

Departure of Armi from Yb bodies requires piRNA precursor loading onto Piwi

I next explored how loss of the RNA-binding activity of Piwi influences the cellular dynamics of Armi in OSCs. To make Piwi defective in RNA binding, we mutagenized the protein based on the previous structural study of Siwi, a PIWI member in silkworm (Matsumoto et al., 2016). The 5'-end of piRNA is recognized by main-chain amino groups in MID domain while the 3'-end is by PAZ domain. Tyr551 in Piwi was mutated to alanine to produce Piwi MID mutant lacking the 5'-end piRNA binding (Figure 26A). Previous study produced Piwi PAZ mutant lacking the 3'-end piRNA binding by mutating Tyr327 and Tyr328 to alanines (Saito et al., 2010). Interestingly, the MID mutant was loaded with neither mature *idelfx*-piRNA nor piRNA precursors, while the PAZ mutant was loaded with precursors, as was Piwi WT control (Figure 26B). I performed the experiments in Zuc-lacking OSCs because under the circumstance the level of Piwi-pre-piRISC was higher than that in normal OSCs (Figure 14A). Endogenous Piwi was also depleted simultaneously to minimize the effect on piRNA precursor-loading onto Flag-Piwi. The level of mature piRNA with Piwi PAZ mutant was much lower than that with Piwi WT. These results corroborated that the 5'-binding pocket in the MID domain,

but not the 3'-binding pocket in the PAZ domain, is crucial for the Piwi-pre-piRISC assembly in OSCs.

Co-immunoprecipitation analysis showed that the PAZ mutant interacted with Armi as efficiently as Piwi WT did, but the MID mutant did not (Figure 27). When the MID mutant was expressed in Zuc-depleted OSCs instead of endogenous Piwi, Armi failed to accumulate on mitochondria (Figure 28A) and was localized to Yb bodies (Figure 28B). When either Piwi WT or the PAZ mutant was expressed instead of the MID mutant, no such phenomenon regarding Armi localization was observed (Figure 28A-B). Both Piwi mutants were detected at Yb bodies (Figure 28B) and had no effect on the expression level of Armi in Zuc-depleted OSCs (Figure 28C). Armi can be localized at Yb body regardless of Piwi mutation in Zuc-expressed cells (Figure 29). These findings suggest that, when Piwi is not bound with piRNA precursors, Armi fails to bind Piwi and resists leaving Yb bodies.

On the basis of these findings and previous ones, I propose that Armi senses pre-piRISC assembly at Yb bodies and translocate together with pre-piRISC to mitochondria (Figure 30). In this way, Armi plays an important role for controlling pre-piRISC translocation.

The short form of two Armi isoforms lacks full-length's N-terminus which is important for piRNA biogenesis

I then explored the molecular function of Armi which is required for pre-piRISC translocation. To prepare a control for the mutant analysis of Armi, I evaluated the behavior of N-terminal Flag-tagged Armi (Flag-Armi). Unexpectedly, Flag-Armi associated with Piwi but not with Gasz (Figure 31A). I then produced C-terminal Flag-tagged Armi (Armi-Flag) and investigated its binding activity with Gasz and Piwi, because it was suspected that N-terminal Flag tag inhibited the interaction between Armi and Gasz. As a result, Armi-Flag has much more interaction with Gasz (Figure 31A). I also confirmed whether N-terminal Flag tag inhibits piRNA production and found that Armi-Flag can rescue piRNA loss induced by endogenous Armi KD but not Flag-Armi (Figure 31B). These findings show the importance of N-terminal regions of Armi in piRNA biogenesis.

Armi is detected as a doublet on western blots (Olivieri et al., 2010; this study). The lower one of the two bands was previously predicted to be an Armi isoform lacking 34 N-terminal amino acids, on the basis of 5' RACE analysis (Olivieri et al., 2010). Two anti-Armi monoclonal antibodies, 2F8A9 and 2D6E11, are now available (Saito et al., 2010; 2D6E11 was produced in the study but remains unreported). Of these, 2F8A9 recognized both Armi bands on western blots, while 2D6E11 recognized solely the upper band (Figure 32A). I expressed Armi WT and the Δ N34

mutant (lacking Met1-Leu34) in endogenous Armi-lacking OSCs individually and performed western blotting probing with the antibodies. 2F8A9 recognized both Armi WT and Δ N34 mutant, while 2D6E11 recognized only WT as expected (Figure 32B). Based on these data, I conclude that the short form of Armi lacks 34 N-terminal amino acids.

Translocation of pre-piRISC from Yb bodies requires the RNA-binding activity and N-terminus of Armi

In this study, I used two Armi mutants; Δ N34 and N756A mutants in order to understand the role of Armi for the translocation of pre-piRISC (Figure 33). N756A is an RNA-binding-defective Armi mutant, given the earlier observation that Asn462 in yeast Upf1 (corresponding to Asn756 in the helicase domain of Armi) was predicted to play a crucial role in the Upf1–RNA interaction on the basis of structural analysis (Chakrabarti et al., 2011). *In vitro* gel shift assay showed that Δ N34 mutant retains an RNA-binding activity but not N756A mutant (Figure 34). Both mutants can be accumulated at Yb body (Figure 35). This result suggests that the localization of Armi itself to and retention at Yb bodies are independent of the RNA-binding activity of Armi. These factors probably depend on Yb–Armi protein–protein interaction (Hirakata et al., 2019). Substitution of endogenous Armi with the

Δ N34 and N756A mutants in OSCs strongly impaired piRNA biogenesis (Figure 36). These results suggest that these mutations disturb the processing after the assembly of Yb bodies.

I then explored whether loss of RNA binding activity and N-terminus of Armi affect its inter-organelle translocation. Immunofluorescence analysis showed that the Δ N34 and N756A mutants do not accumulate on mitochondria and localizes to Yb bodies in Zuc⁻ and Armi-lacking OSCs (Figure 37).

Next, I tested whether the Armi mutant can assemble the trimeric complex with Gasz and Piwi in Zuc-depleted OSCs. To this end, I expressed Armi-Flag Δ N34 and N756A mutants in OSCs where Zuc and Armi were depleted by RNAi and then performed immunoprecipitation. The Armi mutants associated with Piwi as efficiently as Armi WT did, but the ability to interact with Gasz was greatly reduced (Figure 38). This situation was almost identical to that of endogenous Armi in Zuc⁻ and Piwi-lacking OSCs (Figure 21). Moreover, recombinant Armi Δ N34 and N756A mutants maintained the ability to directly interact with Gasz in *in vitro* pull-down assays (Figure 39).

Summarizing the analysis of Armi mutants, loss of RNA-binding activity and N-terminus of Armi inhibits the inter-organelle translocation, but not the Armi-Piwi interaction at Yb body nor the direct interaction with Gasz (Figure 40). These

results suggest that the RNA-binding activity and the N-terminus of Armi are important for its exit from Yb body.

Discussion

Discussion

In this study, I firstly determined the function of Gasz; that is the role as the scaffold protein for Armi-pre-piRISC complex on mitochondria (Figure 41). A recent study showed that Daedalus (Daed), which was identified in the study, anchors the Armi-Piwi complex on mitochondria collaboratively with Gasz in both somatic and germ cells of *Drosophila* ovary (Munafò et al., 2019). Although the domain structure of Daed is similar to that of Gasz, the depletion of only one of them disturbs piRNA biogenesis, indicating they act in a non-redundant manner. Daed appears to be unique to *Drosophilids*, while Gasz is conserved among wide animal species. Why *Drosophilids* requires two scaffold proteins on mitochondria remains unclear.

Interestingly, my study also found the intracellular dynamics of pre-piRISC and the control mechanism for its inter-organelle translocation (Figure 41). In OSCs, transposon-repressing piRISC formation starts with Yb-body formation, which is initiated by multivalent *cis-trans* association between Yb and *flam* RNAs (Hirakata et al., 2019). Other Yb-body components are subsequently incorporated into the bodies in a hierarchical manner: Armi goes in first and then the heterodimer composed of SoYb and Vret joins the body structures. The previous study showed that without Armi, Piwi remains cytosolic and free from

piRNAs (Saito et al., 2010). In the present study, I found that Armi localization to Yb bodies occurs in a Piwi-independent manner. At present, the biological relevance of this hierarchical regulation is unclear. One possibility is that, without Armi, *flam* primary RNA transcripts would not be converted to shorter, secondary precursors. Because Piwi requires 5'-end phosphate of cargo RNAs to load, it is predicted that primary piRNA precursors need to be cleaved by an endonuclease, reducing the levels of pre-piRISC formed at Yb bodies. The nuclease(s) responsible for roughly digesting the primary RNA transcripts to secondary piRNA precursors remains to be identified. The processor creating secondary piRNA precursors (*i.e.*, creating 5' ends of the precursors for Piwi binding) from primary RNA transcripts may be identified from Armi partners.

Armi senses pre-piRISC assembly at Yb body and triggers the exit of the complex from Yb bodies (Figure 41). Why is such multilayered, elaborate regulation required in piRISC processing? One possible reason is that Yb, but not Armi, Zuc, or even Piwi, has a strong sequence preference in RNA binding (Ishizu et al., 2015; Ishizu et al., 2019). To control this situation where the selectivity of piRNA precursor is completely due to Yb, OSCs might employ Yb as the core factor of Yb-body formation [because of the propensity to form LLPS-driven multivalent concentrates (Yb bodies) when bound with huge *flam* RNA transcripts] and

decide to use Yb bodies as the site for Arm1 to induce pre-piRISC formation and quality control before the complex heads to mitochondria where piRISC maturation finally occurs. A recent study reported that Arm1 has 5'-to-3' RNA-unwinding activity and it is thought to contribute relaxing single-strand piRNA precursors avoiding the formation of the secondary structure because Zuc can process only ssRNAs (Nishimasu et al., 2012). In this way, the *flam*-piRNA precursors are securely bound with Arm1 and Piwi, achieving the production of transposon-repressing piRISC.

In this study, I also revealed the molecular function of Arm1 in the inter-organelle translocation. Loss of the N-terminus and RNA-binding activity of Arm1 severely inhibited pre-piRISC translocation (Figures 40-41). The finding support an interesting idea that the departure of pre-piRISC from Yb bodies, prior to its relocation to mitochondria, depends on the RNA-binding activity of Arm1. This type of regulation relying on the RNA-binding activity of Arm1 is biologically relevant because Arm1 without RNA-binding activity would fail to unwind (relax) piRNA precursors for Zuc cleavage, blocking piRNA biogenesis. The regulation would provide major help in avoiding this mismanagement. Another potential reason for relying on Arm1's RNA-binding activity might be related to Arm1's promiscuous RNA binding (Ge et al., 2019; Ishizu et al., 2019). When Arm1 is already

bound with pre-piRISC via piRNA precursor, after leaving Yb bodies Armi would not be able to bind to other cellular RNAs at random. Thus, it is very important for maintaining the integrity of piRNA biogenesis in OSCs to ensure that the pre-piRISC departure from Yb bodies occurs only after Armi associates with pre-piRISC via both Piwi and piRNA precursor.

The Armi mutant defective in RNA binding was able to interact with Piwi, indicating the interaction is through protein–protein interaction (Figure 38A). However, Armi failed to associate with Piwi when Piwi was devoid of piRNA precursors (Figure 27). These findings suggest that conformational change of Piwi occurs before and after its piRNA precursor loading and that Armi is sensitive to the conformational alteration of Piwi. Surprisingly, even after Armi successfully bound to pre-piRISC via piRNA precursor, the lack of Armi's only 34 N-terminal residues blocked the release of the complex from the bodies (Figure 40). Although at present the role of the N-terminus remains unknown, if it were revealed, this would be very helpful to understand in more detail the molecular flow and regulation of the piRISC processing pathway.

Conclusion

Conclusion

In this study, I determined the function of Gasz; that is the role as the scaffold protein for Armi–pre-piRISC complex on mitochondria for Zuc-dependent piRNA maturation. Interestingly, my study also found the intracellular dynamics of pre-piRISC and the control mechanism for its inter-organelle translocation. Pre-piRISC is formed in an Armi-dependent manner and Armi senses the assembly at Yb body and triggers the exit of the complex from Yb bodies. Furthermore, I found that the N-terminus and the RNA-binding activity of Armi are required for the departure of Armi from Yb body. In this way, piRNA processing is under the strict control between two organelles; the one is Yb body, which is the place for piRNA precursor selection, and the other is mitochondria, which is the place for piRNA maturation. I think that these molecular mechanisms contribute to quality control for piRNA biogenesis in order to avoid process wrong RNA substrate into piRNAs.

piRNA biogenesis occurs at RNA–protein granules like Yb bodies and mitochondria in most animals. I believe that these molecular mechanisms found in my study lead to understand inter-organelle piRNA processing in many animals.

Figures

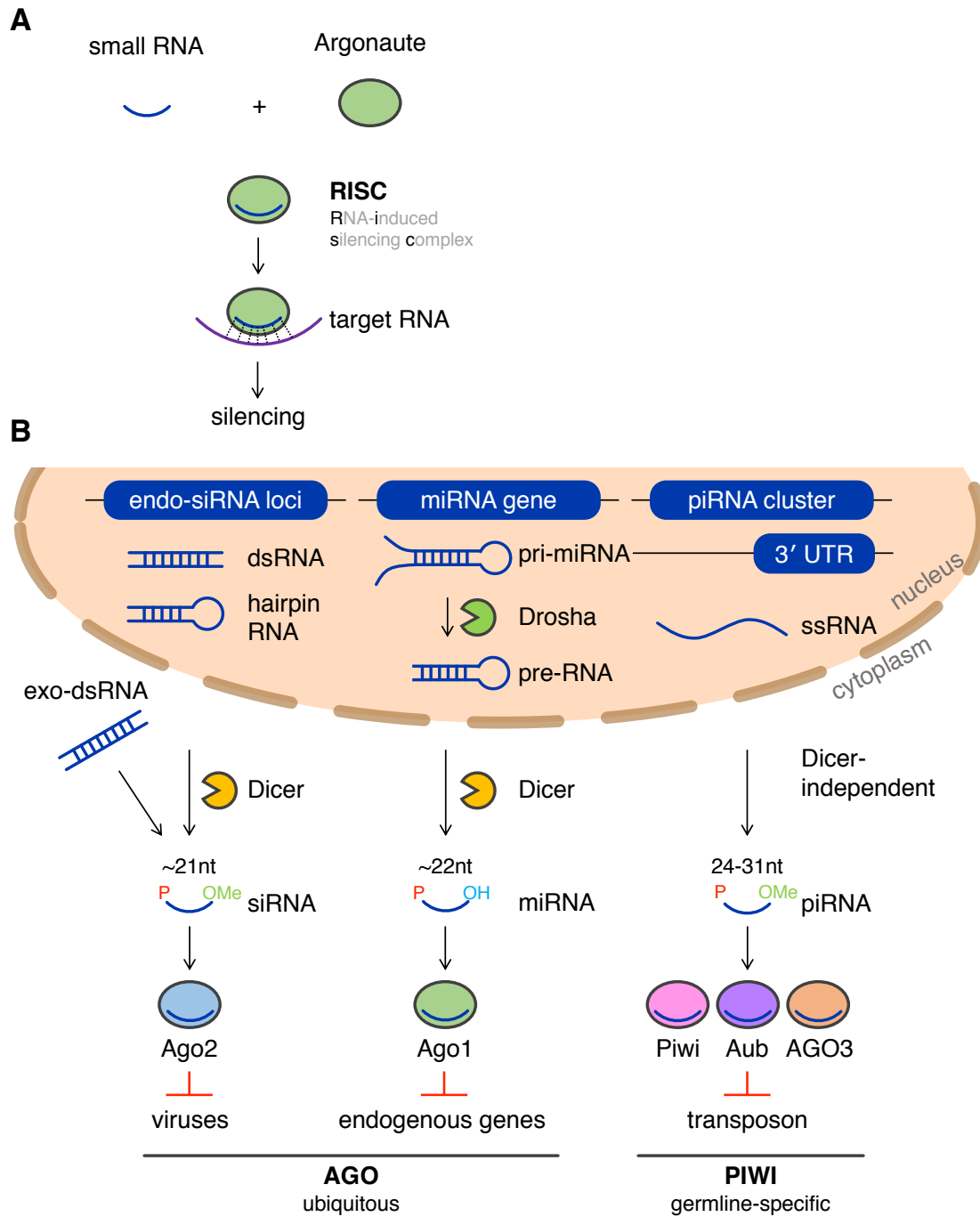


Figure 1 (legend on next page).

Figure 1 RNA silencing mechanism in *Drosophila*

(A) The outline of RNA silencing mechanism (B) siRNAs (~21 nt long), both endogenous and exogenous, are produced from precursors by an RNase III ribonuclease Dicer, and form a RISC with Ago2. siRNAs target mainly viruses. miRNAs (~22 nt long) are produced from their own precursors transcribed from miRNA genes depending on two RNase III ribonucleases, Drosha and Dicer, in a sequential manner. miRNAs form RISC with Ago1. miRNAs target endogenous genes. piRNAs (24–31 nt long) arise from RNA transcripts transcribed from piRNA clusters via complex piRNA biogenesis machinery. Some piRNAs are derived from protein-coding mRNAs, particularly their 3'-untranslated regions (UTR), although their target genes remain unknown. piRNAs form piRISCs with PIWI proteins, Piwi, Aub and Ago3, to repress transposons.

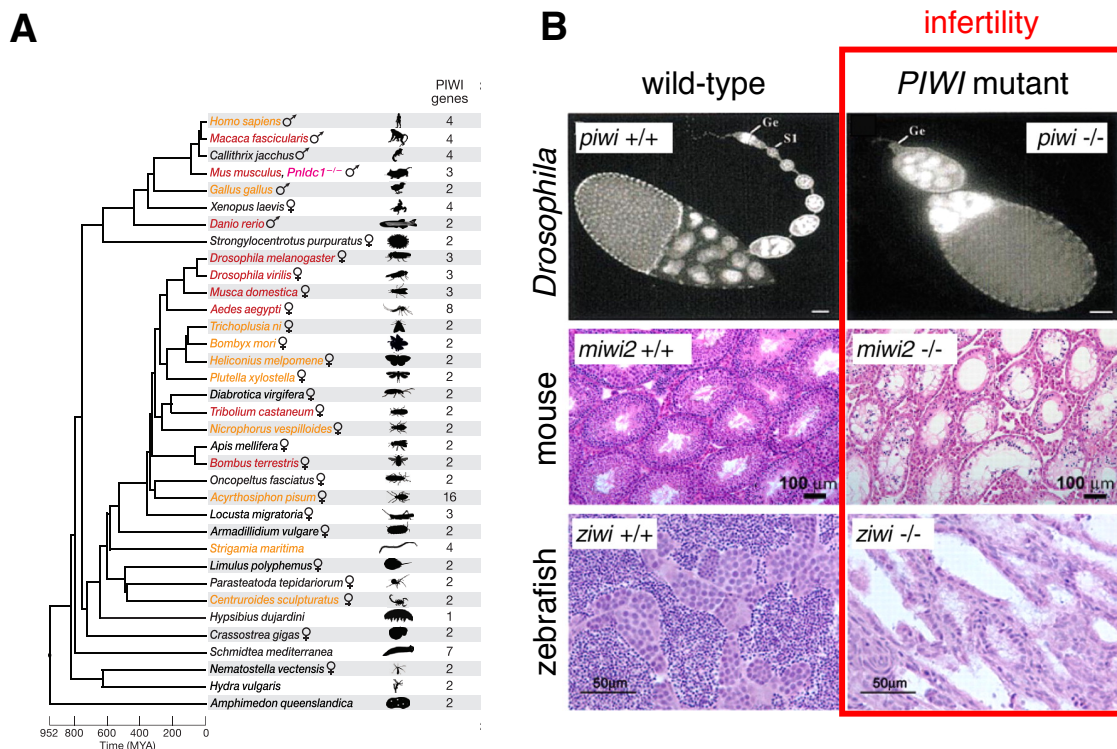


Figure 2. The evolutionary conservation of piRNA pathway among animals

(A) This figure is modified from Gainetdinov et al., 2018. Cladogram of a representative set of animal species indicating the approximate time of each divergence. PIWI genes are widely conserved among animals although the number of PIWI members are various. (B) This figure is modified from Klattenhoff and Theurkauf 2008. The mutation of PIWI genes leads to loss of gonadal development and fertility. *miwi2* and *ziwi* are homologues of *piwi*.

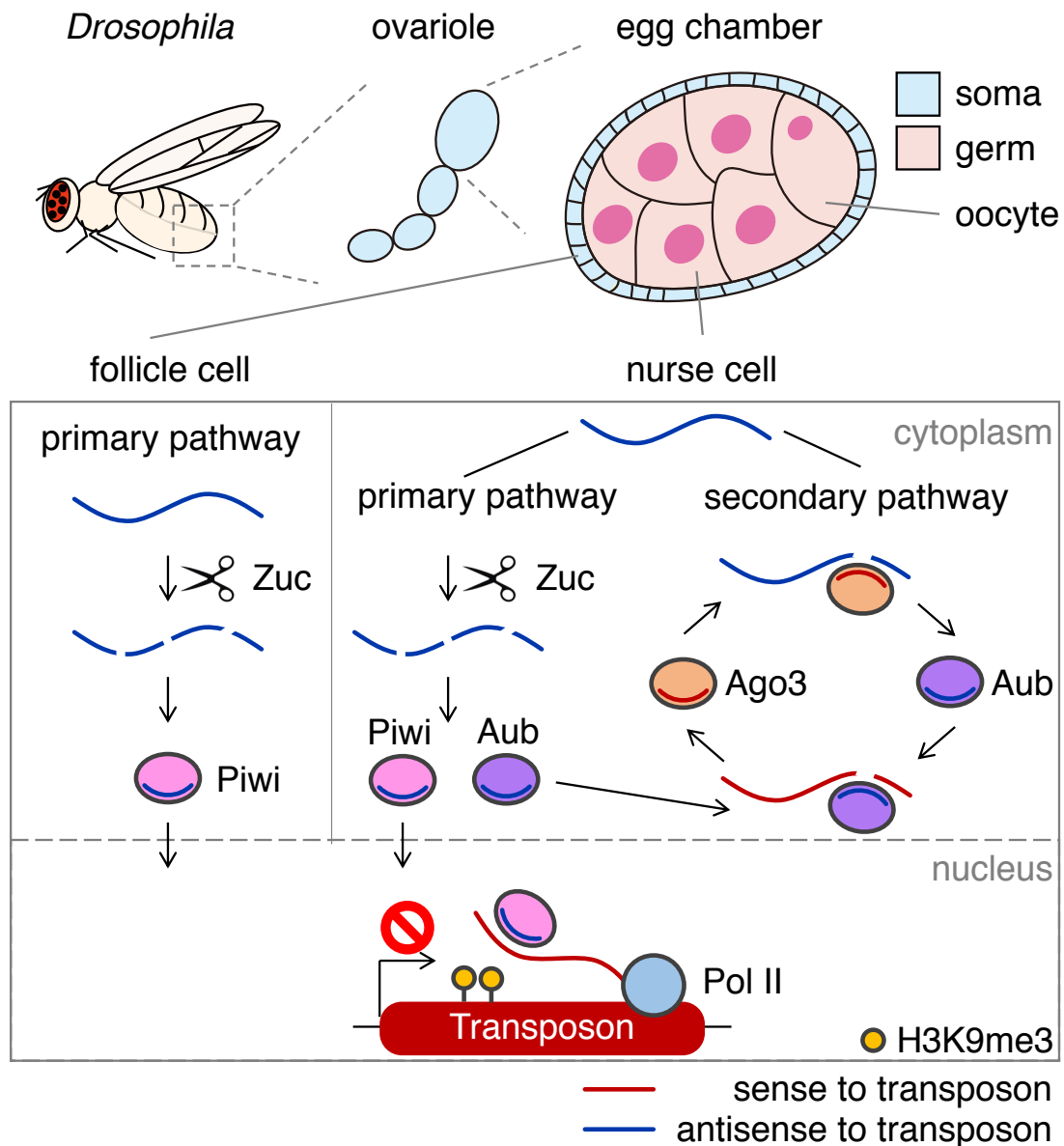


Figure 3. piRNA pathway in *Drosophila*

Drosophila ovaries contain egg chambers at different stages of development. Egg chambers are composed of germ cells (an oocyte and 15 nurse cells; pink) and somatic follicle cells (light blue) which surround them. The expression patterns of PIWI proteins and the mechanisms of piRNA biogenesis and transposon silencing are distinct in somatic and germ cells.

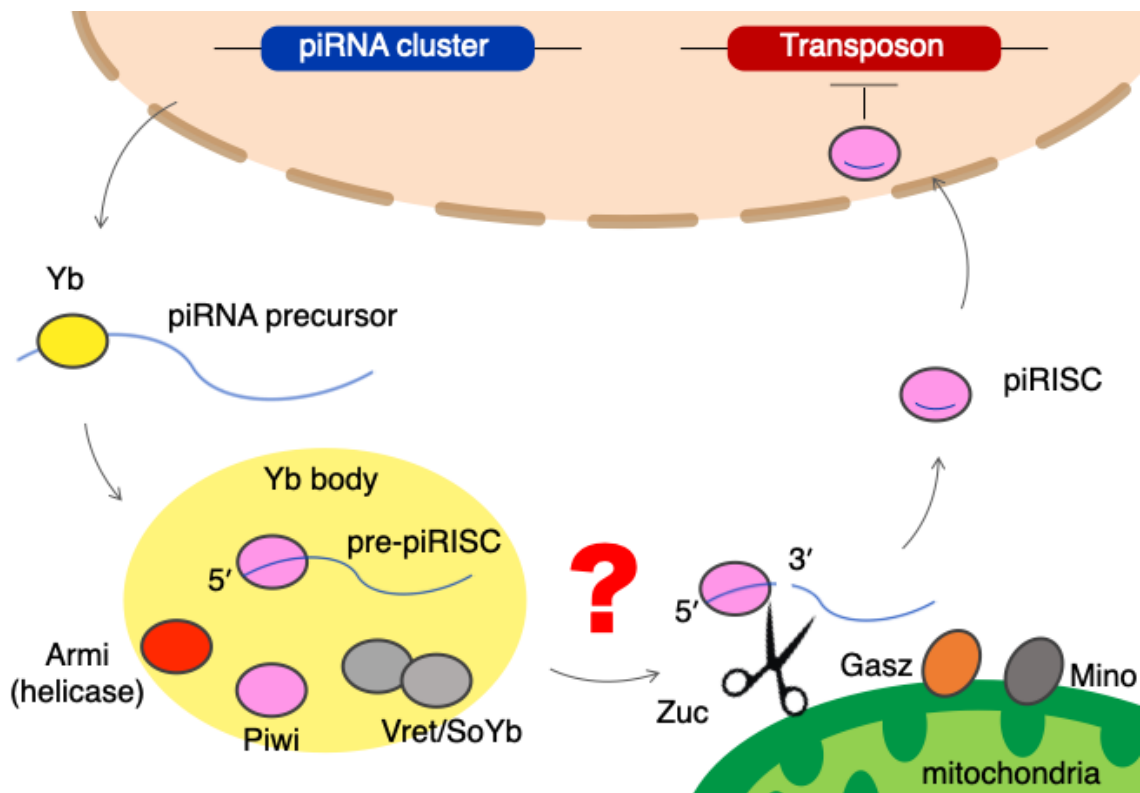


Figure 4. The current model of piRNA biogenesis in *Drosophila* ovarian somatic cells

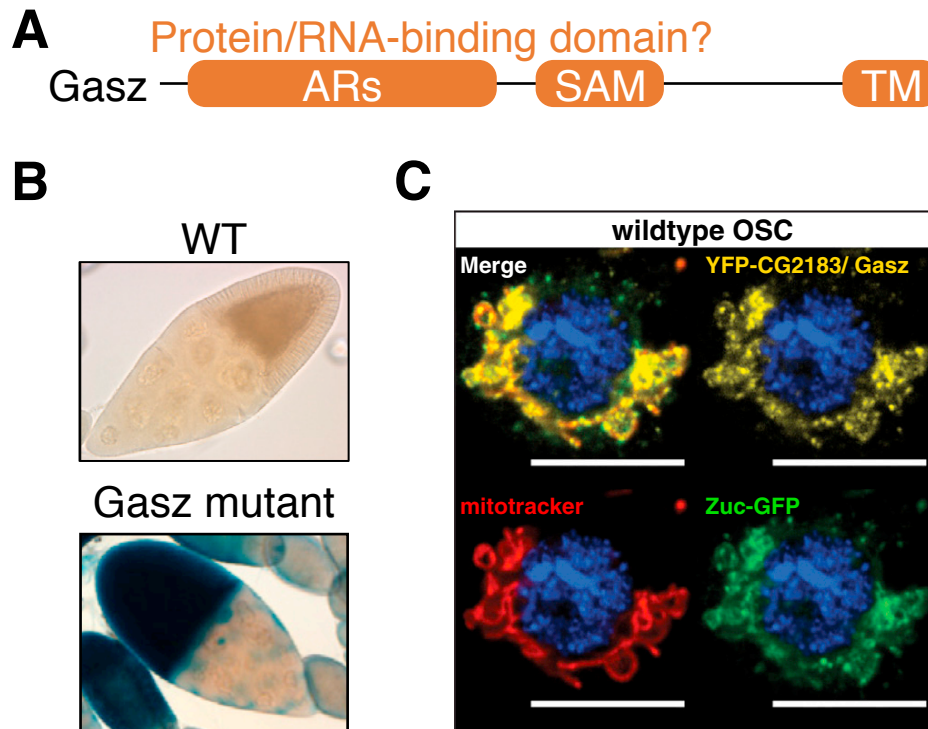


Figure 5. The mitochondrial factor Gasz is essential for piRNA pathway in *Drosophila*

(A) The domain organization of Gasz AR; Ankyrin repeats, SAM; Sterile alpha motif domain, TM; transmembrane region. AR and SAM domain are considered to function as protein- or RNA-binding domains (Kim and Bowie 2003; Li et al., 2006; Mosavi et al., 2004). (B) This figure is modified from Handler et al., 2013. The mutation of Gasz induces the derepression of transposon in *Drosophila* egg chambers. Transposon expressions are visualized by using LacZ-reporter and β -gal staining. (C) This figure is modified from Handler et al., 2013. Ectopically expressed Gasz (yellow) as well as Zuc (green) is localized on mitochondria in OSCs. Mitochondria (red) are stained by mitotracker.

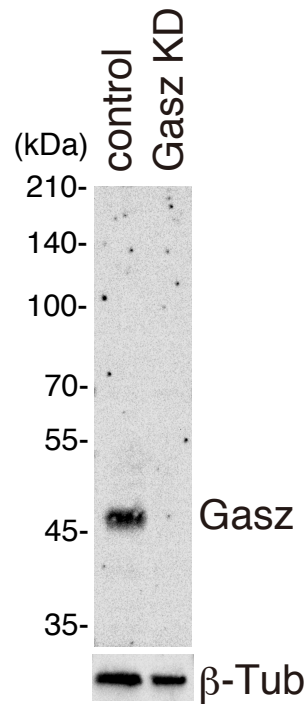


Figure 6. Antibodies produced in this study

Western blotting was performed for OSC cell lysates using anti-Gasz monoclonal antibody produced in this study. β -Tubulin is detected as a loading control.

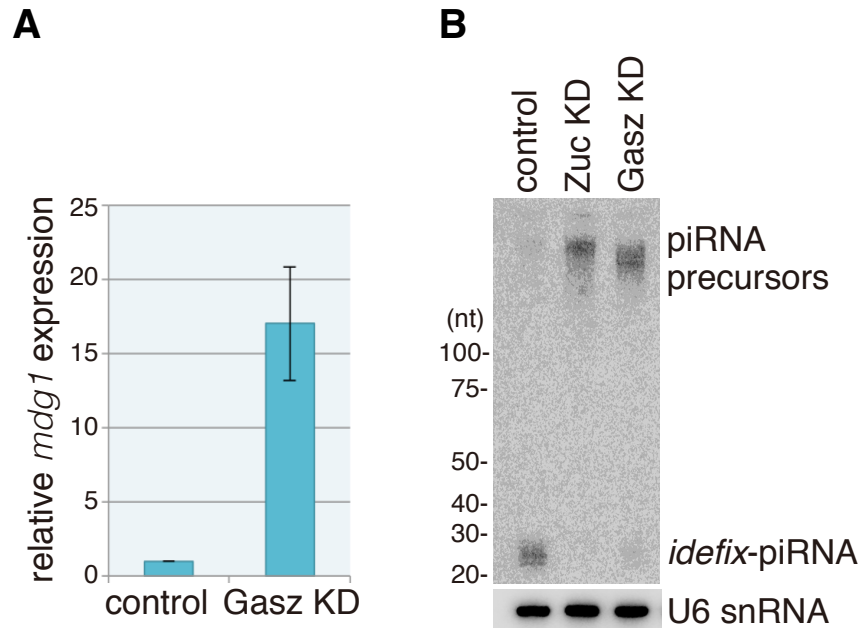


Figure 7. Gasz is essential for Zuc-dependent piRNA biogenesis
 (A) Depletion of Gasz leads to transposon derepression. The expression level of *mdg1* transposon was monitored by qRT-PCR. Values were averaged and normalized to the expression level of the ribosomal protein gene (*rp49*). Bars and error bars represent mean \pm standard error of the mean (SEM) values of three independent experiments. (B) Northern blotting shows that Gasz depletion (Gasz KD) led to the accumulation of *flam*-piRNA precursors but reduced the level of mature *idexfix*-piRNA arising from the *flam*-piRNA precursors, as in the case of Zuc depletion (Zuc KD). U6 snRNA was detected as a loading control.

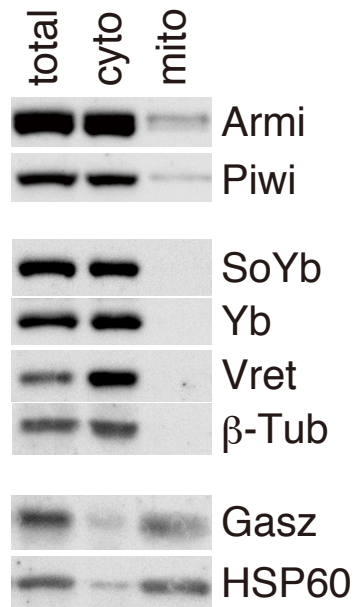


Figure 8. Armii and Piwi are detected in mitochondrial fraction of OSCs

Western blotting showing the protein levels of endogenous Armii, Piwi, SoYb, Yb, Vret, and Gasz in total OSC lysate (total), the mitochondrial fraction (mito), and the cytoplasmic fraction after mitochondrial isolation (cyto). β -Tubulin (β -Tub) and HSP60 were detected as markers for the “cyto” and “mito” fractions, respectively.

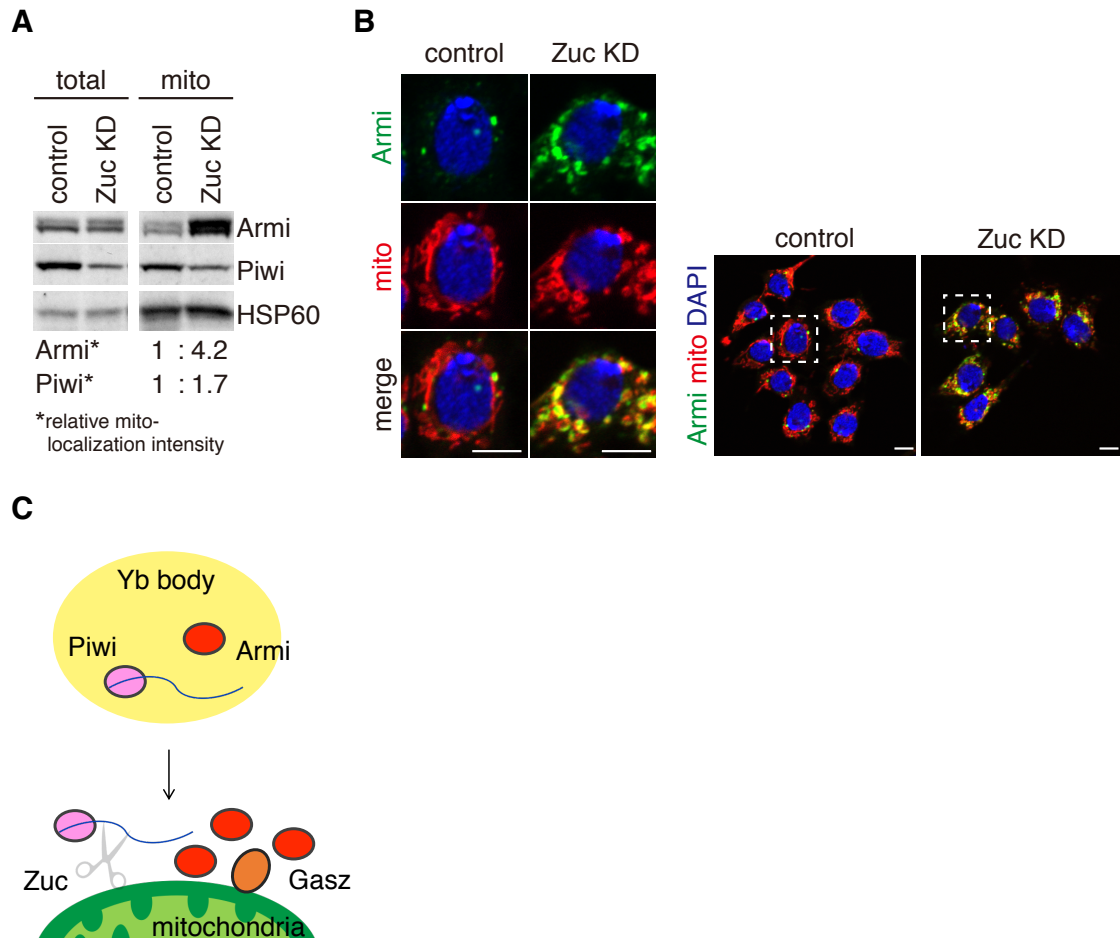


Figure 9 (legend on next page).

Figure 9. Armi aberrantly accumulates on mitochondria in the absence of Zuc

(A) Western blotting comparing the abundances of Armi and Piwi in total OSC lysate (total) and the mitochondrial fraction (mito) before (control) and after (Zuc KD) Zuc knockdown in OSCs. Relative mito-localization intensity (*) shows the band intensity of proteins in “mito” normalized by the band intensity of proteins in “total” and HSP60. (B) Left: Immunofluorescence shows that the Armi signal (green) is strongly overlapped with the mitochondrial signal (red) in Zuc-depleted OSCs (Zuc KD). Armi is localized to Yb bodies and cytosol in control OSCs (control). The signals of cytosol are hard to detect because the highest signal is regulated not to saturate. The scale bar represents 5 μ m. DAPI (blue) shows the nuclei. Right: Larger immunostaining views of the cell images shown in Left. The cells appeared in the left figure are boxed with white broken line. (C) Armi is aberrantly accumulated on mitochondria upon Zuc depletion.

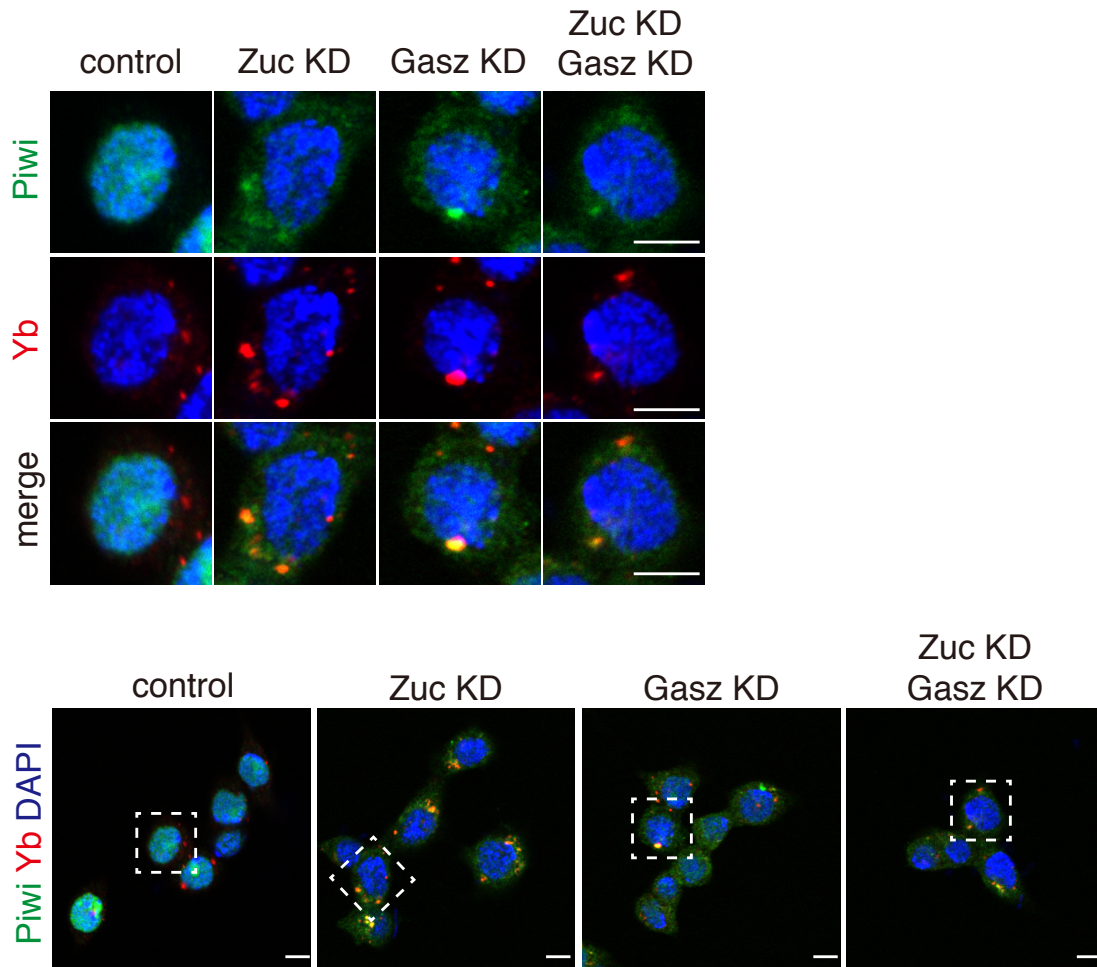


Figure 10. The cellular localization of Piwi in Zuc and Gasz-depleted OSCs

Upper: Localization of Piwi (green) in OSCs upon Zuc and Gasz depletion. Yb bodies are shown in red. Lower: Larger immunostaining views of the cell images shown in upper panels. The cells appeared in the upper panels are boxed with white dotted line. Piwi was mislocalized in the cytosol upon loss of Zuc and/or Gasz. Some fraction of Piwi was detected at Yb bodies as has previously been reported (Saito et al., 2010). The scale bar represents 5 μm . DAPI (blue) shows the nuclei.

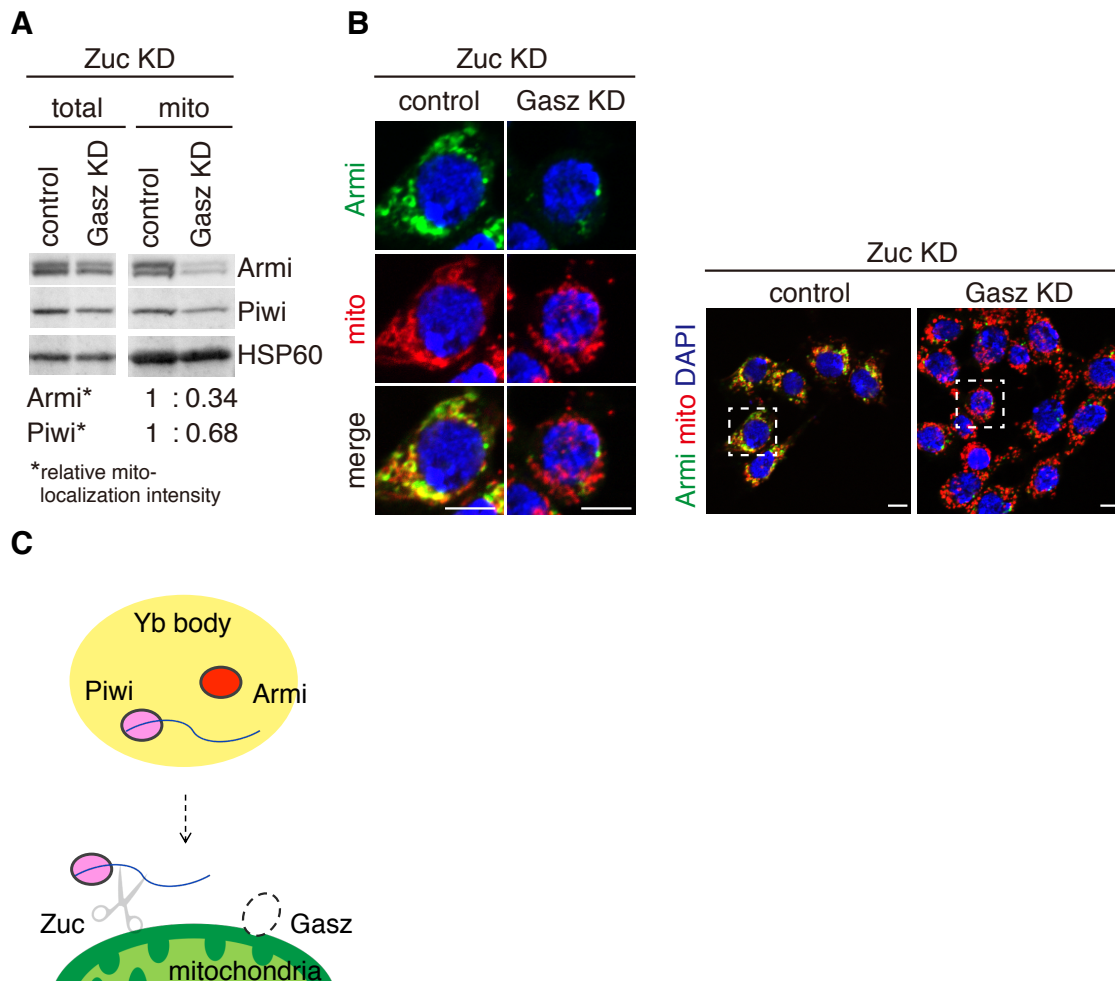


Figure 11 (legend on next page).

Figure 11. Armi does not accumulate on mitochondria upon Gasz loss in Zuc-depleted OSCs

(A) Western blotting comparing the abundances of Armi and Piwi in total OSC lysate (total) and the mitochondrial fraction (mito) before (control) and after (Gasz KD) Gasz depletion in Zuc-depleted OSCs (Zuc KD). Relative mito-localization intensity (*) shows the band intensity of proteins in “mito” normalized by the band intensity of proteins in “total” and HSP60. (B) Immunofluorescence shows that the Armi mitochondrial signal (green) found in Zuc-depleted cells (Zuc KD/control) mostly disappeared after additional Gasz depletion in the cells (Zuc KD/Gasz KD), but was found at Yb bodies. The signals of cytosol are hard to detect because the highest signal is regulated not to saturate. Mitochondrial signal is shown in red. The scale bar represents 5 μ m. DAPI (blue) shows the nuclei. (C) Armi cannot translocate from Yb body to mitochondria upon Gasz-depletion.

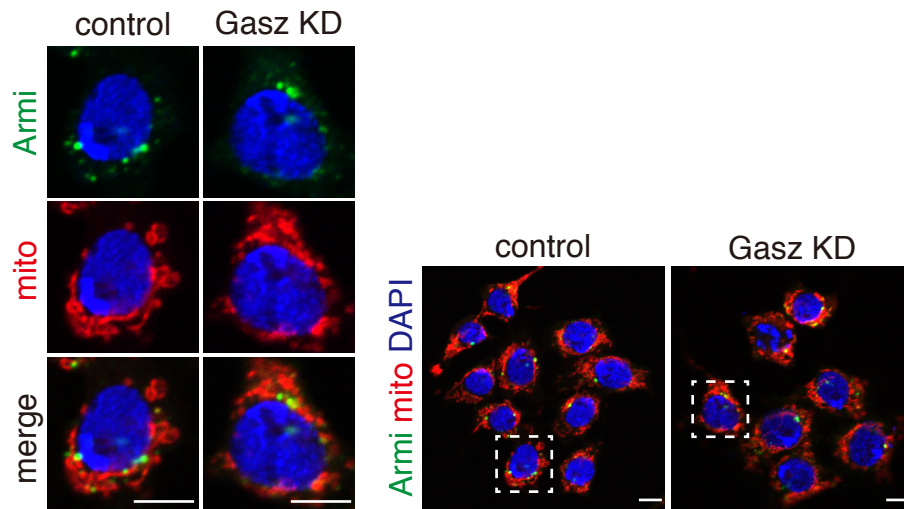


Figure 12. Armi is localized at Yb body even after Gasz depletion
 Left: Localization of Armi (green) in OSCs upon Gasz depletion. Mitochondria are shown in red. Right: Larger immunostaining views of the cell images shown on the left. The scale bar represents 5 μm . DAPI (blue) shows the nuclei.

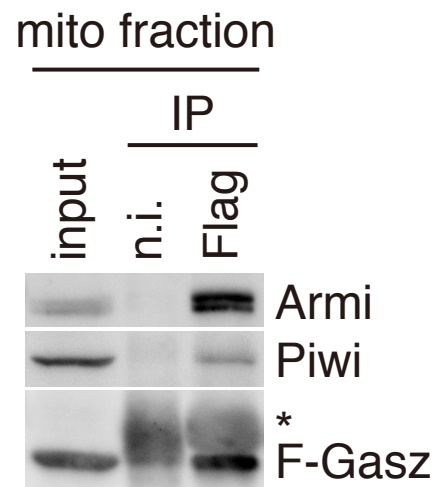


Figure 13. Gasz binds with Armi and Piwi on mitochondria

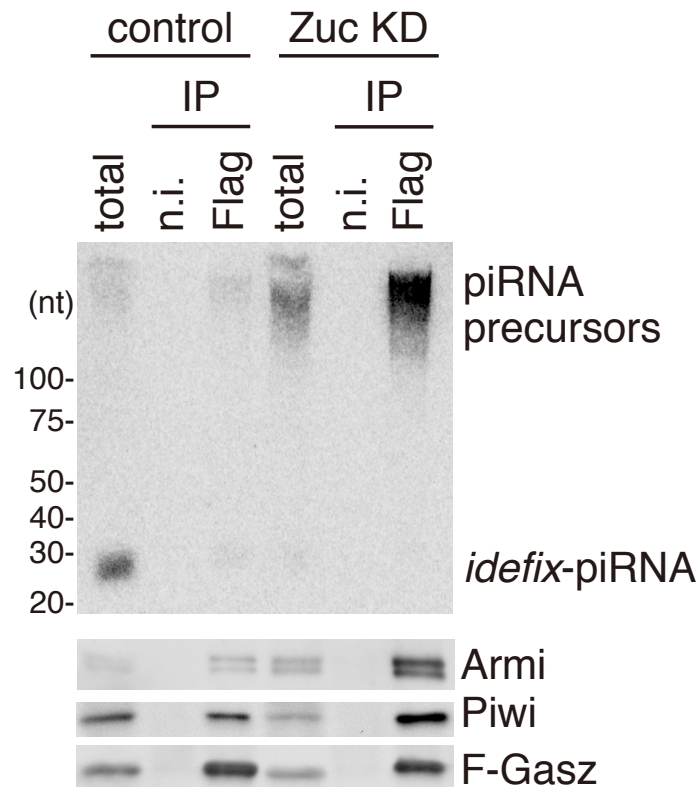


Figure 14. The abundance of Arm–Piwi–pre-piRISC in the Gasz complex increases upon Zuc depletion.

Upper: Northern blotting shows that the *flam*-piRNA precursors in the Flag-Gasz complex (Flag) accumulated upon Zuc depletion (Zuc KD). Lower: Co-immunoprecipitation from whole-cell lysate of OSCs before (control) and after (Zuc KD) Zuc depletion and subsequent western blotting show that the levels of Piwi and Arm in the Flag-Gasz (F-Gasz) complex increased upon Zuc depletion (Zuc KD).

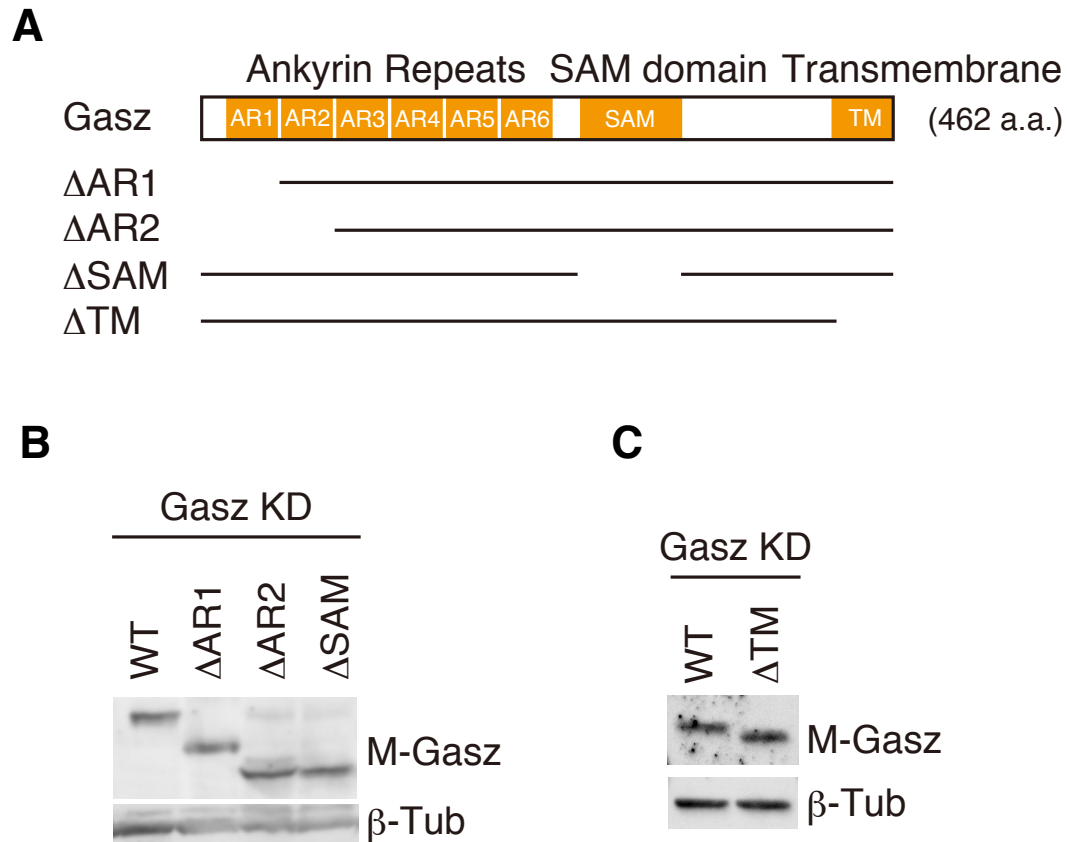


Figure 15. The Gasz mutants used in this study

(A) Domain structures of Gasz deletion mutants used in this study. (B and C) The expression levels of Myc-Gasz (M-Gasz) WT and mutants in Gasz-depleted OSCs (Gasz KD). β -Tubulin (β -Tub) was detected as a loading control.

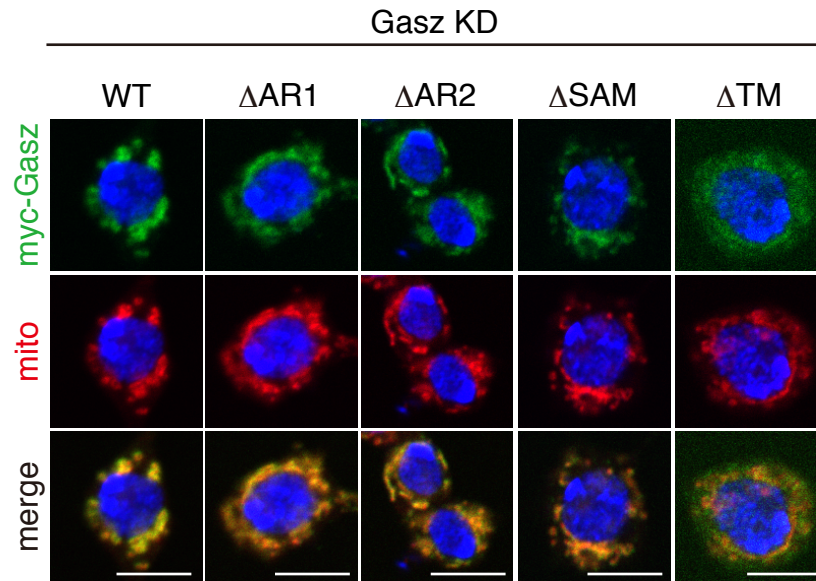


Figure 16. The cellular localization of Gas2 deletion mutants
 Δ AR1, Δ AR2, Δ SAM Myc-Gas2 (M-Gas2) mutants (green), were localized on mitochondria (red) as well as WT, while Δ TM mutant was dispersed to cytosol. The scale bar represents 5 μ m. DAPI (blue) shows the nuclei.

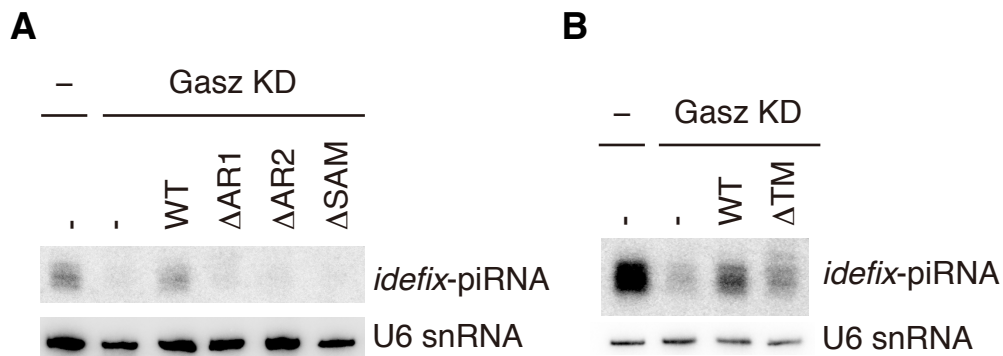


Figure 17. ARs, SAM domain and mitochondrial localization of Gasz are important for piRNA biogenesis.

(A and B) Northern blotting shows that siRNA-resistant WT Myc-Gasz (M-Gasz), but not deletion mutants, rescued the defects in *idefix*-piRNA production caused by endogenous Gasz depletion. U6 snRNA was used as a loading control.

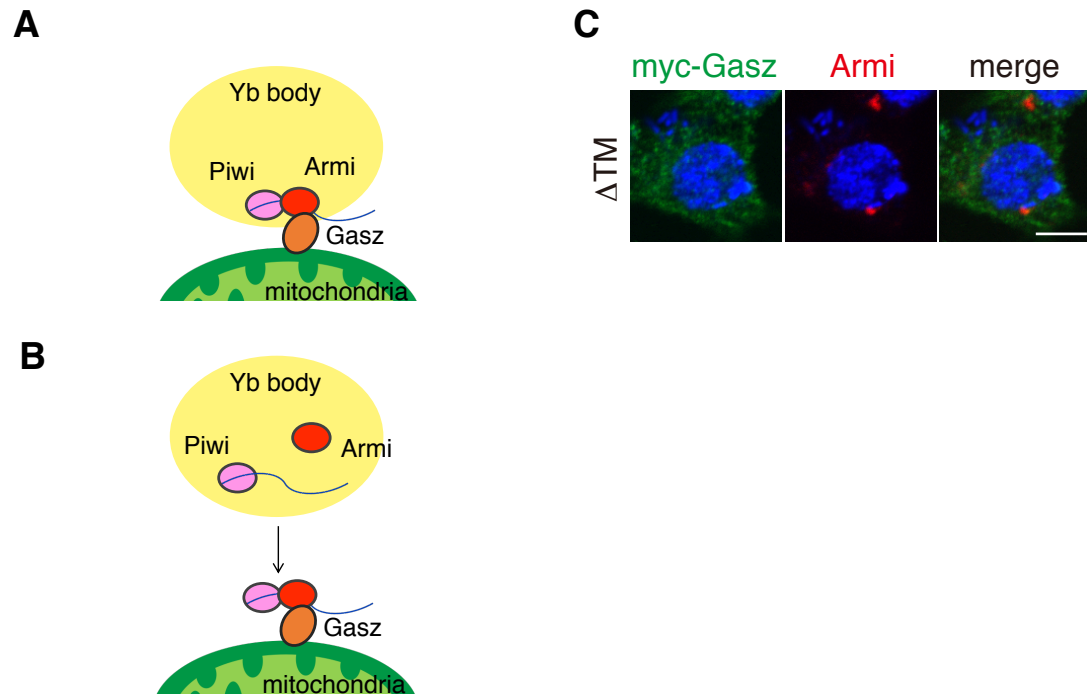


Figure 18. Gasz interacts with Armi which is dispatched from Yb body.

(A and B) Two possibilities about the interaction with Gasz and Armi. (C) $\Delta TM1$ mutant did not accumulate with Armi which is at Yb body.

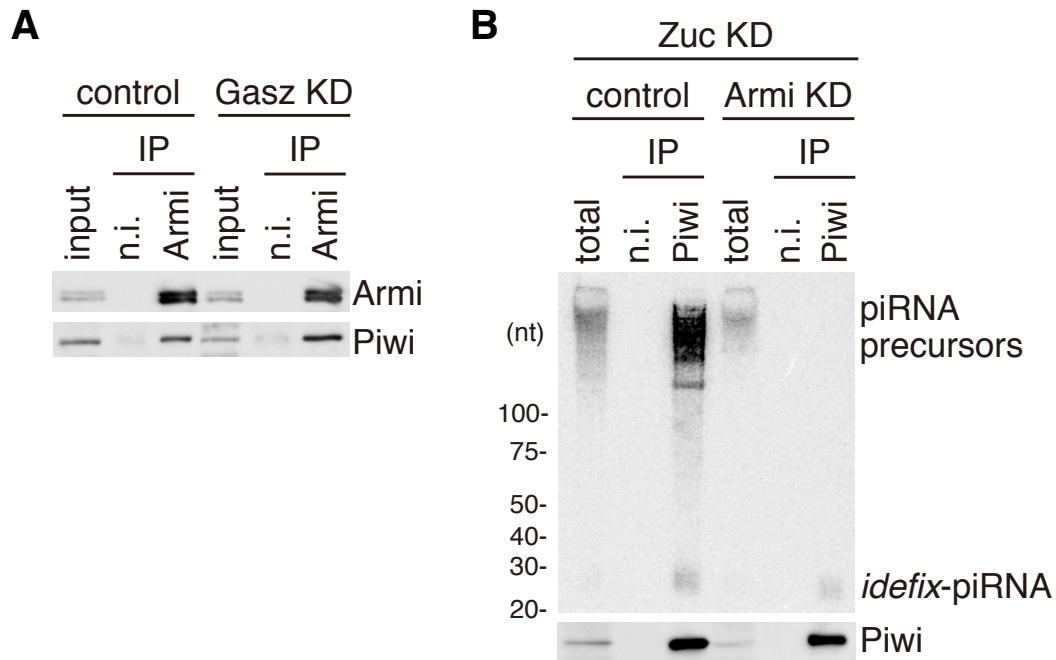


Figure 19. pre-piRISC is formed in an Armi-dependent manner
 (A) The Piwi–Armi interaction remained stable even after Gasz depletion. (B) Upper: The *flam*-piRNA precursors associated with Piwi disappeared upon Armi depletion (Armi KD) in Zuc-lacking OSCs (Zuc KD). Zuc KD was performed to make it easy to detect piRNA precursors. Lower: The abundance of immunopurified Piwi is shown by western blotting.

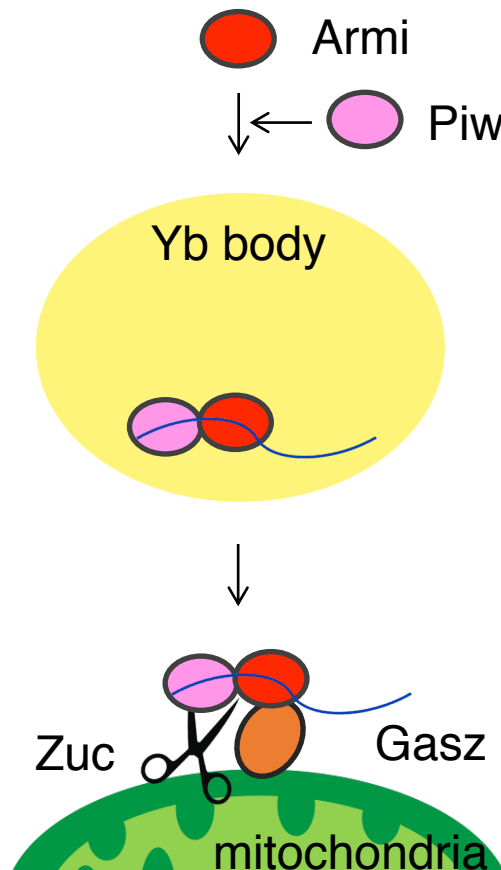


Figure 20. pre-piRISC is formed at Yb bodies in an Armi-dependent manner and the complex is translocated together to mitochondria for Zuc-dependent maturation.

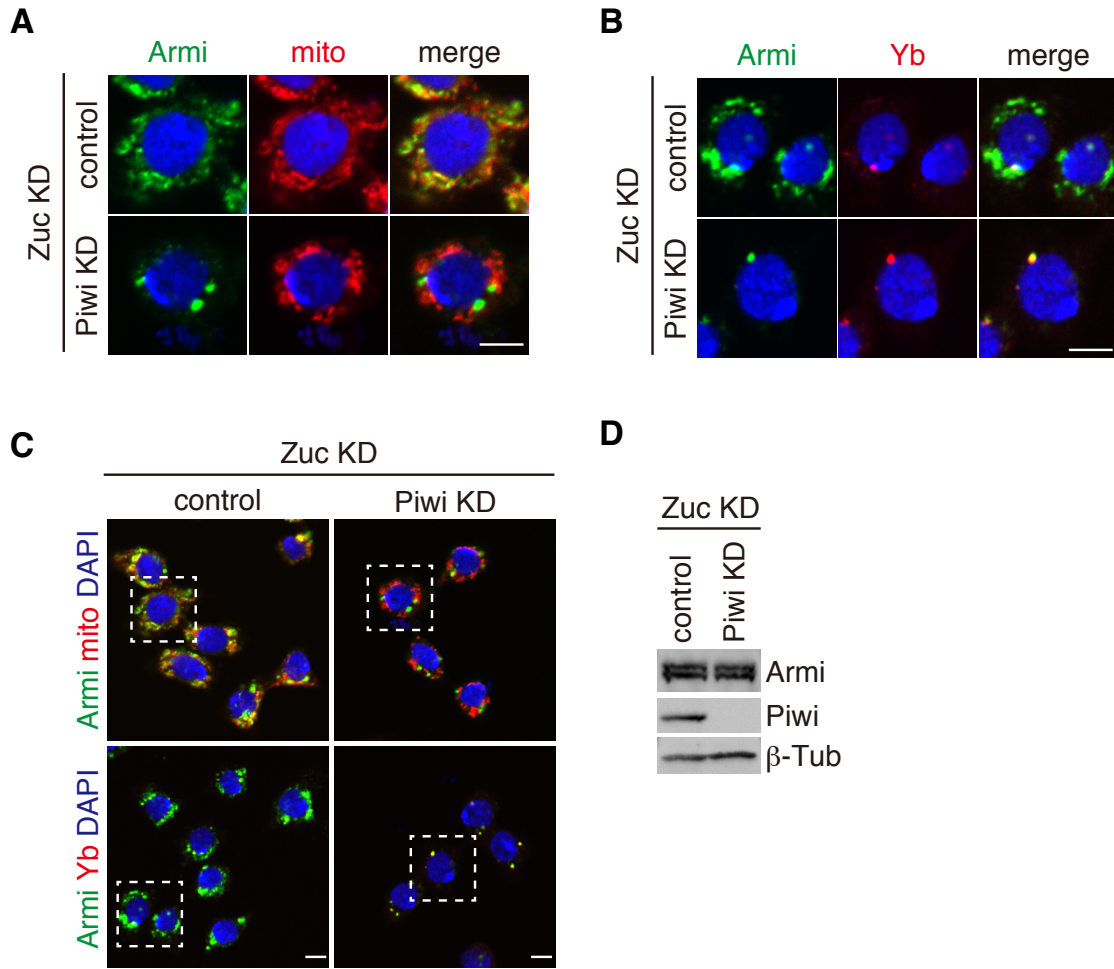


Figure 21. The aberrant mitochondrial accumulation of Armi induced by Zuc loss was completely released upon additional Piwi depletion

(A and B) Depletion of endogenous Piwi (Piwi KD) in Zuc-lacking OSCs (Zuc KD) caused Armi (green) to remain to be Yb bodies. Localization of Armi at Yb bodies is shown in (B). Mitochondrial (A) and Yb (B) signals are shown in red. The scale bar represents 5 μ m. DAPI (blue) shows the nuclei. (C) Larger immunostaining views of the cell images shown in (A) and (B). The cells appeared in the upper figures are boxed with white broken line. Armi behaved similarly in the cells other than the one shown in (A) and (B). The scale bar represents 5 μ m. (D) Piwi depletion hardly affected the level of Armi in Zuc-depleted OSCs. β -Tubulin (β -Tub) was detected as a loading control.

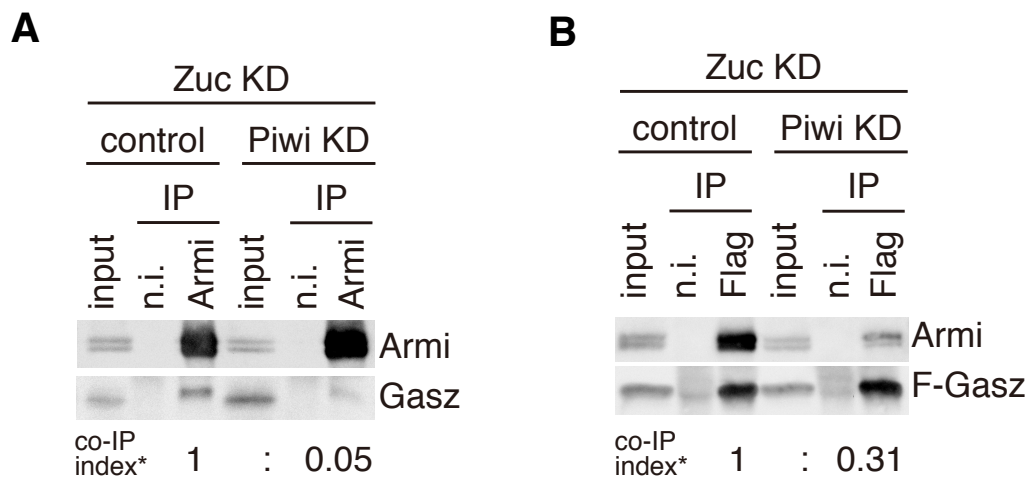


Figure 22. Armi no longer stably associated with Gasz upon Piwi depletion

(A) The Armi complex was immunopurified from Zuc-lacking OSCs (Zuc KD) before (control) and after (Piwi KD) Piwi depletion and probed for detecting Armi and Gasz. Armi no longer stably associated with endogenous Gasz upon Piwi depletion in Zuc-lacking OSCs. Co-IP index (*) shows that the ratio of Gasz intensity in the Armi complex isolated from Zuc-depleted cells (Zuc KD/control) and Zuc- and Piwi-depleted cells (Zuc KD/Piwi KD) is 1:0.05. (B) The Flag-Gasz (F-Gasz) complex was immunopurified from Zuc-lacking OSCs (Zuc KD) before (control) and after (Piwi KD) Piwi depletion and probed for detecting Armi and F-Gasz. F-Gasz was ectopically expressed prior to immunoprecipitation. Co-IP index (*) shows that the ratio of Armi intensity in the F-Gasz complex isolated from Zuc-depleted cells (Zuc KD/control) and Zuc- and Piwi-depleted cells (Zuc KD/Piwi KD) is 1:0.31.

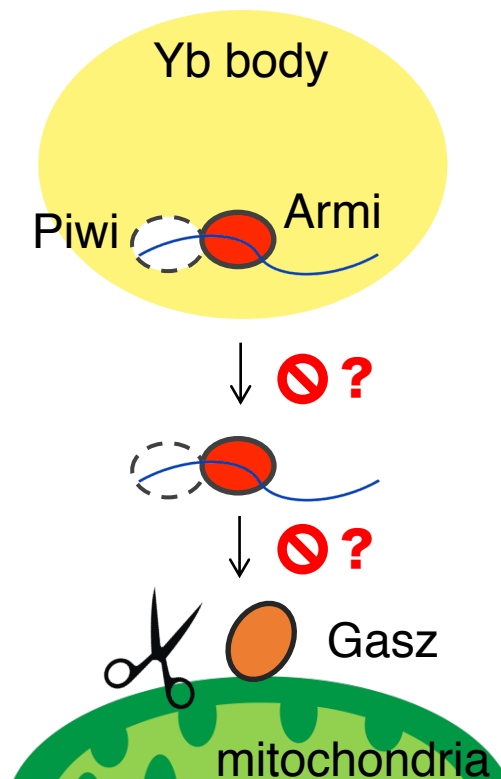


Figure 23. Two scenarios to explain the situation upon Piwi depletion

Without Piwi, (1) Armi resists leaving Yb bodies and thus is stuck there, or (2) Armi leaves Yb bodies and moves to mitochondria but cannot remain there, possibly because of loss of the ability to attach to Gasz.

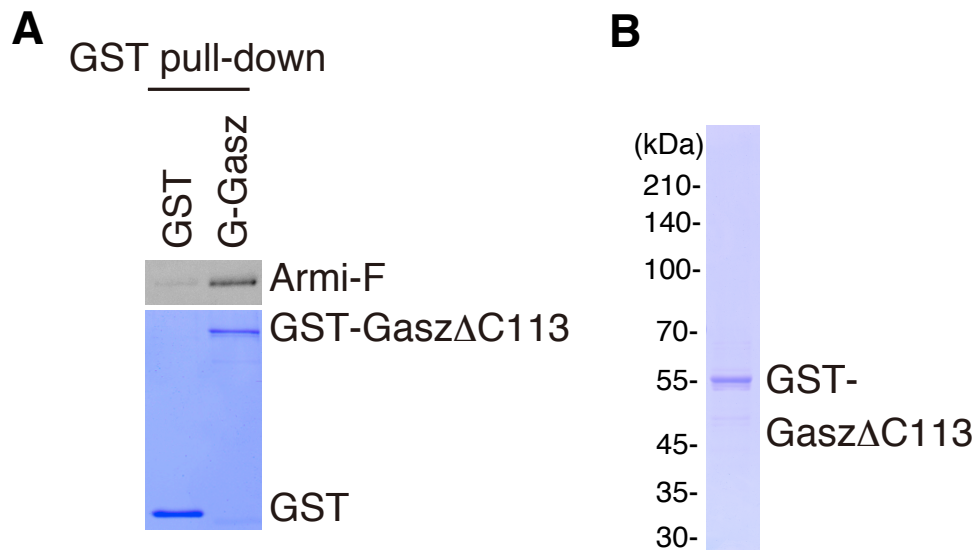


Figure 24. Gasz has direct interaction with Armi

(A) *In vitro* pull-down assays show that Armi-Flag (Armi-F) directly binds with GST-GaszΔC113 but hardly with GST. Armi-F was immunopurified from Schneider 2 (S2) cells under harsh conditions. GST and GST-GaszΔC113 were visualized by CBB staining, while Armi-F was detected by western blotting using anti-Flag antibodies. (B) Purified recombinant GST-Gasz (ΔC113 lacking Leu349-Ser461 containing the TM region at the C-terminus) used in the experiment shown in A. The protein was stained with CBB.

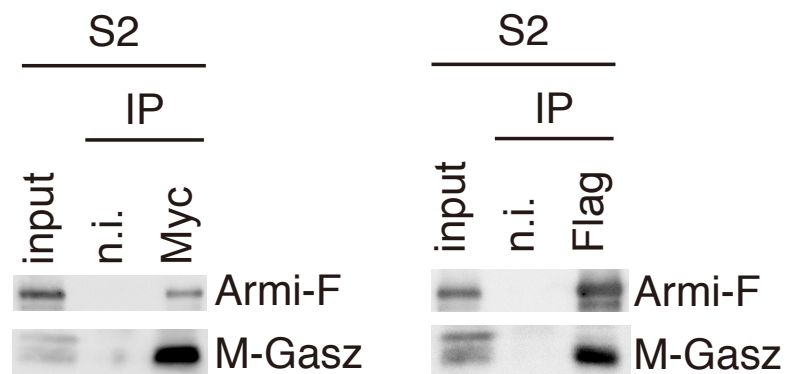


Figure 25. Gasz has interaction with Armi in S2 cells.

Myc-Gasz (M-Gasz) and Armi-Flag (Armi-F) interacted with each other in Schneider 2 (S2) cells. Left immunoprecipitation experiment was performed using an anti-Myc antibody, while Right was using an anti-Flag antibody.

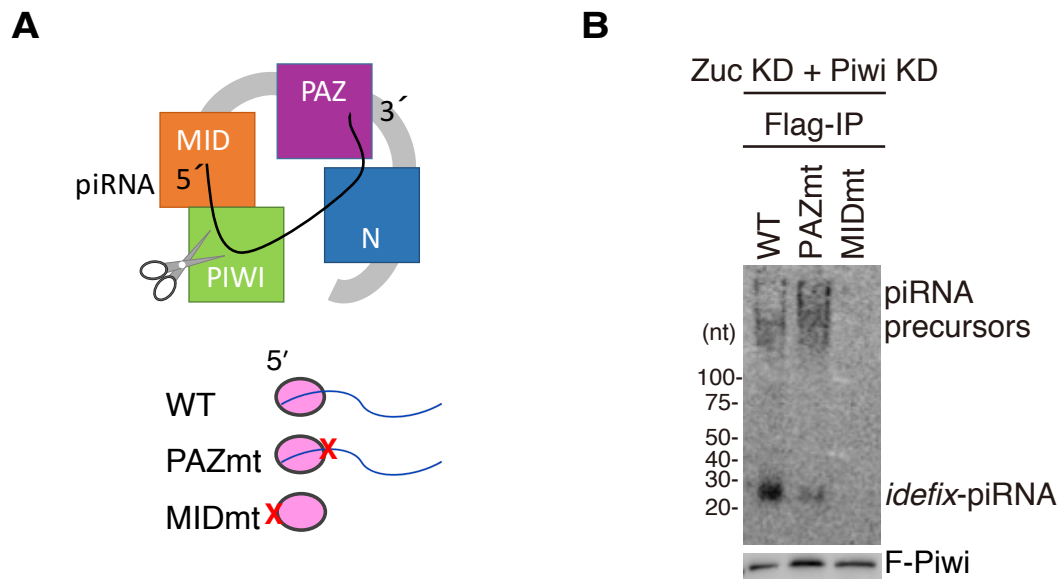


Figure 26. 5'-end recognition by MID domain is important for the assembly of pre-piRISC.

(A) Upper: The structure of Siwi: a PIWI member in silkworm (Matsumoto et al., 2016) Lower: Piwi mutants used in this study. (B) Upper: Northern blotting shows that Flag-Piwi (F-Piwi) WT (WT) and PAZ mutant (PAZmt) but not MID mutant (MIDmt) bound with *flam*-piRNA precursors in Zuc-depleted OSCs. Endogenous Piwi was depleted simultaneously with Zuc (Zuc KD + Piwi KD). Zuc was depleted by RNAi and so residual Zuc may have remained in cells. Therefore, a tiny amount of piRNAs was loaded onto Piwi. F-Piwi WT, PAZmt, and MIDmt were made to be RNAi-resistant by mutagenesis. Lower: The abundance of immunopurified F-Piwi is shown by western blotting.

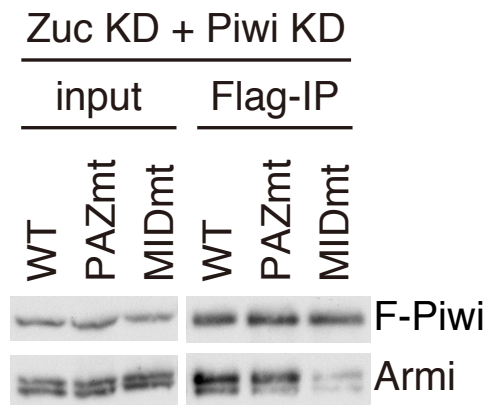


Figure 27. The Piwi PAZ mutant interacts with Armi as efficiently as Piwi WT does, but the MID mutant does not.

Western blotting shows that Flag-Piwi (F-Piwi) WT (WT) and PAZ mutant (PAZmt) but not MID mutant (MIDmt) bound with Armi in Zuc/Piwi-depleted OSCs (Zuc KD + Piwi KD).

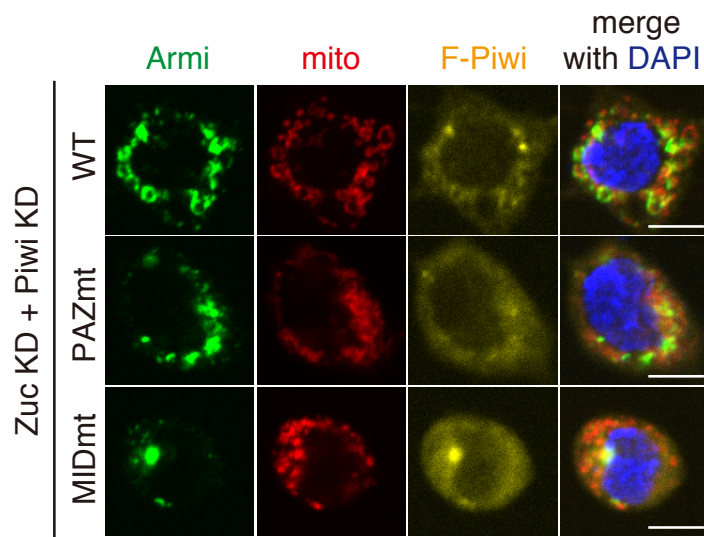
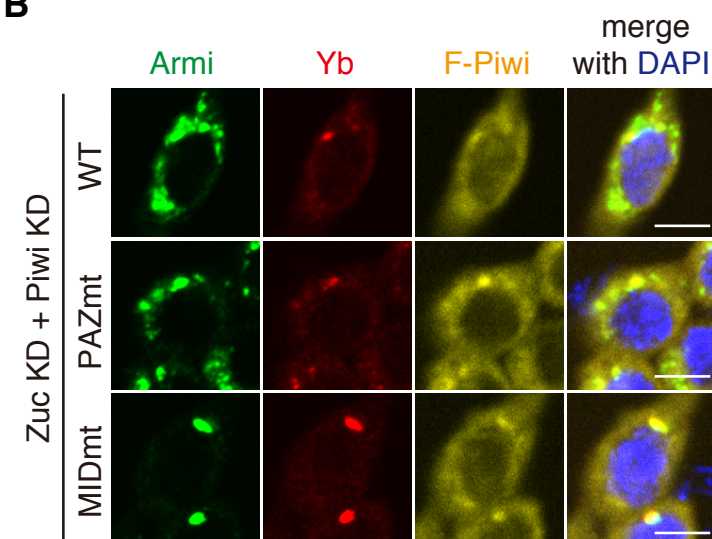
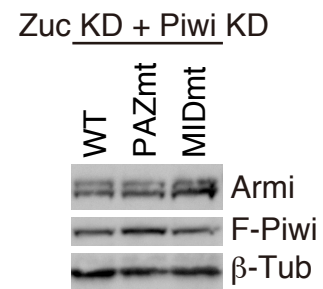
A**B****C****Figure 28** (legend on next page).

Figure 28. Armi fails to translocate to mitochondria when Piwi is not bound with piRNA precursors

(A and B) Armi localization to Yb bodies observed in Zuc⁻ and Piwi-depleted OSCs (Zuc KD + Piwi KD) was restored by ectopic expression of Flag-Piwi WT and PAZ mutant (PAZmt) but not of MID mutant (MIDmt). Armi, mitochondria, and F-Piwi are shown in green, red, and yellow, respectively. Co-localization with Yb (red) is shown in B. The scale bar represents 5 μ m. DAPI (blue) shows the nuclei. (C) The expression levels of Flag-Piwi (F-Piwi) WT and PAZ/MID mutants (PAZmt/MIDmt) in Zuc/Piwi-depleted OSCs (Zuc KD + Piwi KD). β -Tubulin (β -Tub) was detected as a loading control.

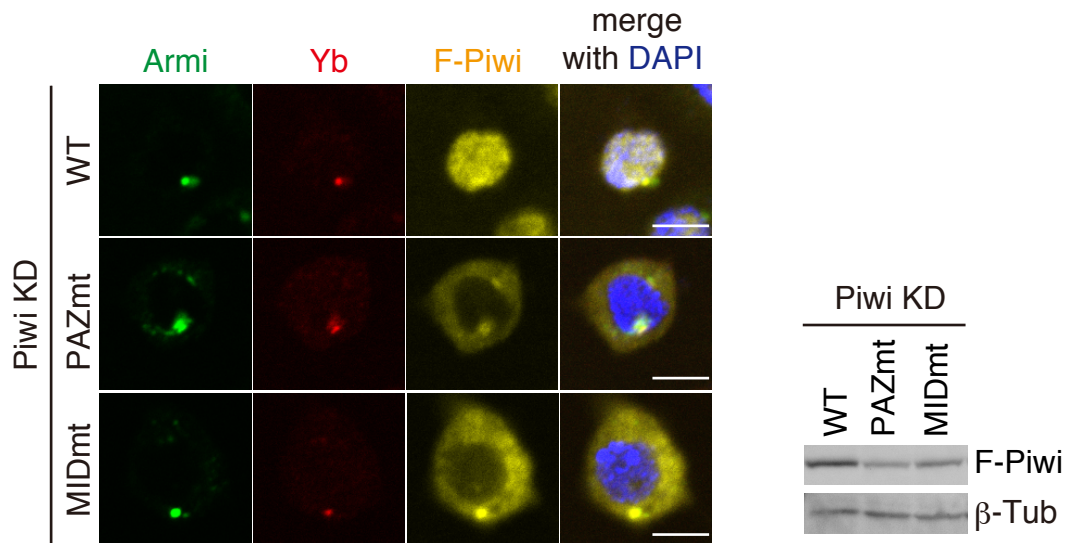


Figure 29 The behaviors of Piwi mutants in Zuc-expressed cells
 Left; The cellular localization of Flag-Piwi (F-Piwi) WT and PAZ/MID mutants (PAZmt/MIDmt) (yellow), Yb (red), and Armi (green) in Piwi-depleted OSCs (Piwi KD). The scale bar represents 5 μ m. DAPI (blue) shows the nuclei. Right; The expression levels of Flag-Piwi (F-Piwi) WT and PAZ/MID mutants (PAZmt/MIDmt) in Piwi-depleted OSCs (Piwi KD). β -Tubulin (β -Tub) was detected as a loading control.

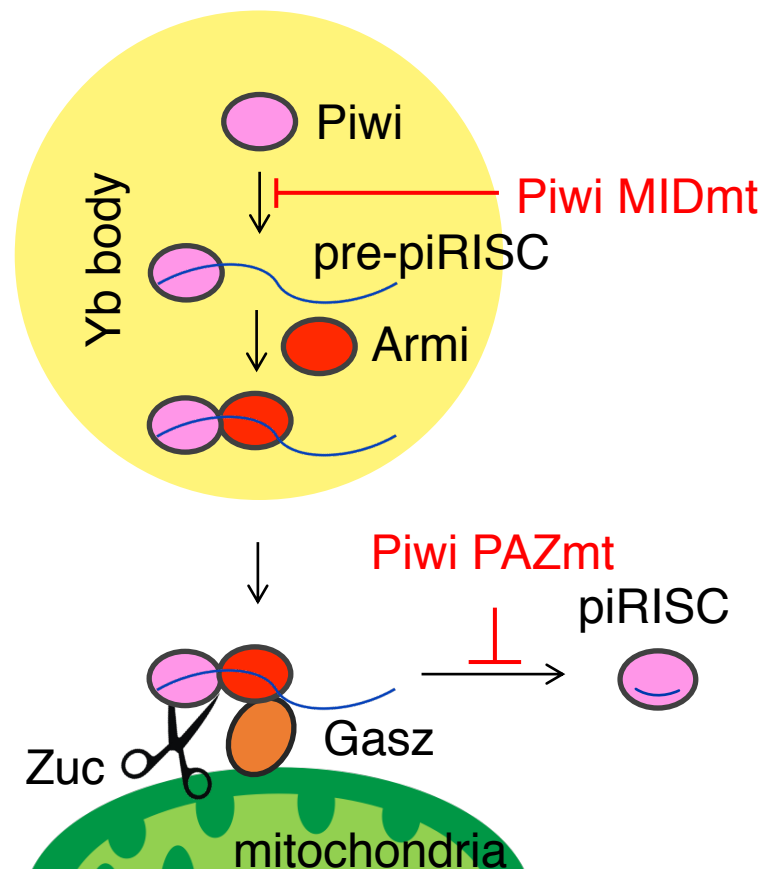


Figure 30. Armi senses Piwi-pre-piRISC assembly at Yb bodies and translocates together with Piwi-pre-piRISC to mitochondria.

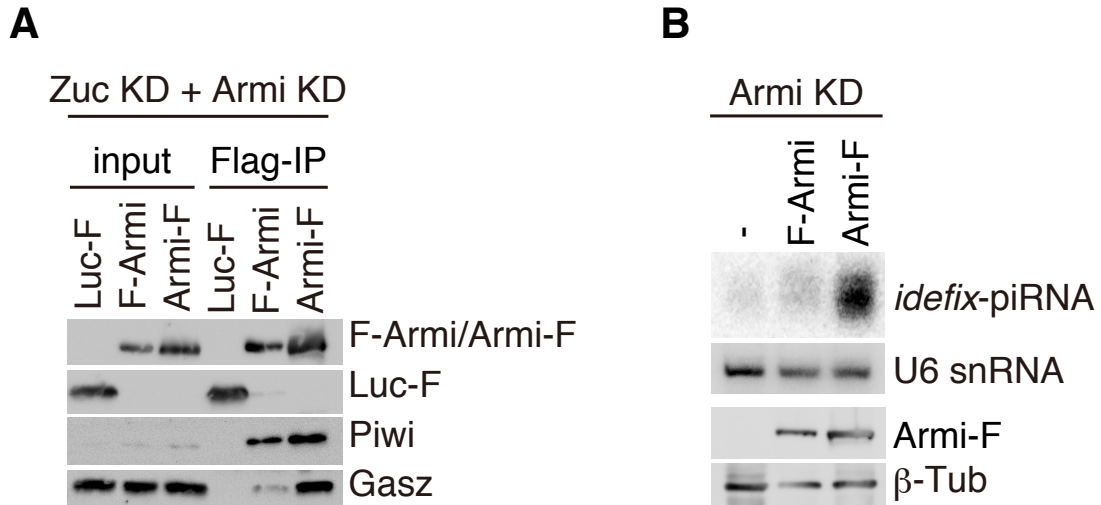


Figure 31. Addition of Flag-tag to the N-terminus of Armi inhibits piRNA biogenesis.

(A) Immunoprecipitation and subsequent western blotting shows that Armi-Flag (Armi-F) but not Flag-Armi (F-Armi) strongly bound with Gasz in Zuc/Armi-depleted OSCs (Zuc KD + Armi KD). Piwi bound with both Armi (F-Armi and Armi-F). Luciferase-Flag (Luc-F) was used as a negative control. (B) Upper: Northern blotting shows that siRNA-resistant WT Armi-Flag (Armi-F), but not Flag-Armi (F-Armi), rescued the defects in *idefix*-piRNA production caused by endogenous Armi depletion. U6 snRNA was used as a loading control. Lower: The expression levels of Armi-Flag (Armi-F) and Flag-Armi (F-Armi). β -Tubulin was used as a loading control.

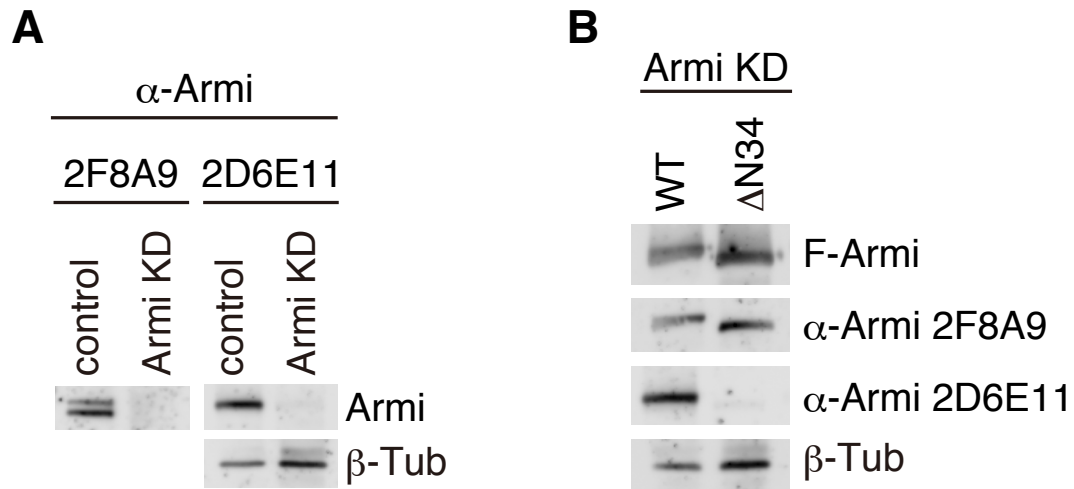


Figure 32. The short form of Armi isoforms lacks the N-terminus
 (A) Anti-Armi antibody 2F8A9 recognized both Armi bands on western blots, while 2D6E11 recognized solely the upper band. The signals of 2F8A9 were stripped away and then the same membrane was reprobed with 2D6E11. β -Tubulin (β -Tub) was detected as a loading control. (B) Western blotting showed that 2F8A9 anti-Armi antibody recognized both Armi-Flag (Armi-F) WT and Δ N34 mutant, while 2D6E11 recognized only WT. β -Tubulin (β -Tub) was detected as a loading control.



Figure 33. The domain structure of Armi mutants used in this study

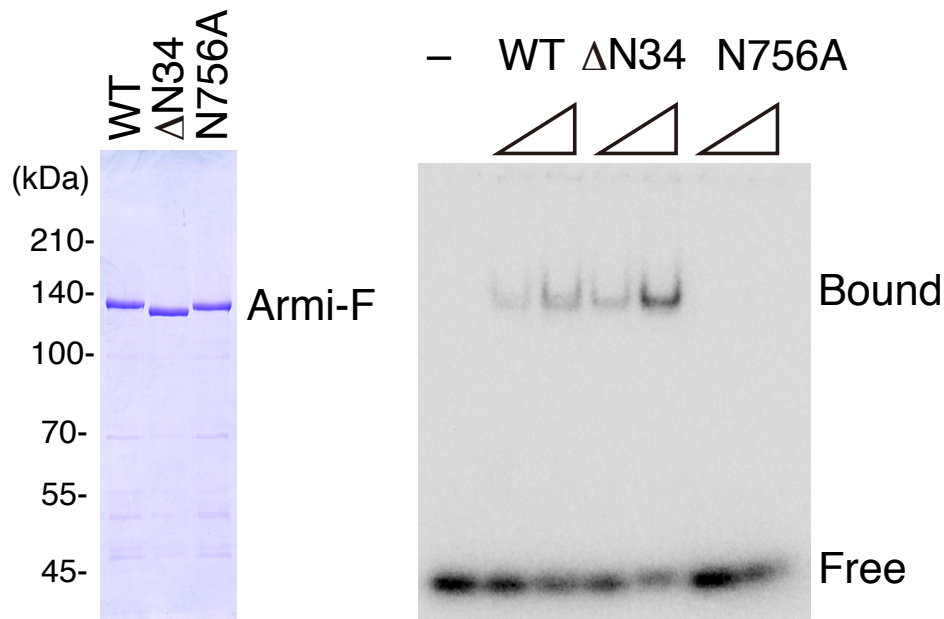


Figure 34. Armi WT and Δ N34 mutant have RNA-binding activity but not N756A mutant.

Left: Purified recombinant Armi-Flag (Armi-F) WT and mutants (Δ N34 and N756A) used in the experiment. Right: RNA-binding activity of Armi-Flag WT, Δ N34, and N756A. Here, 16-nt single-stranded RNA was 5'-end-labeled and incubated with Armi-Flag.

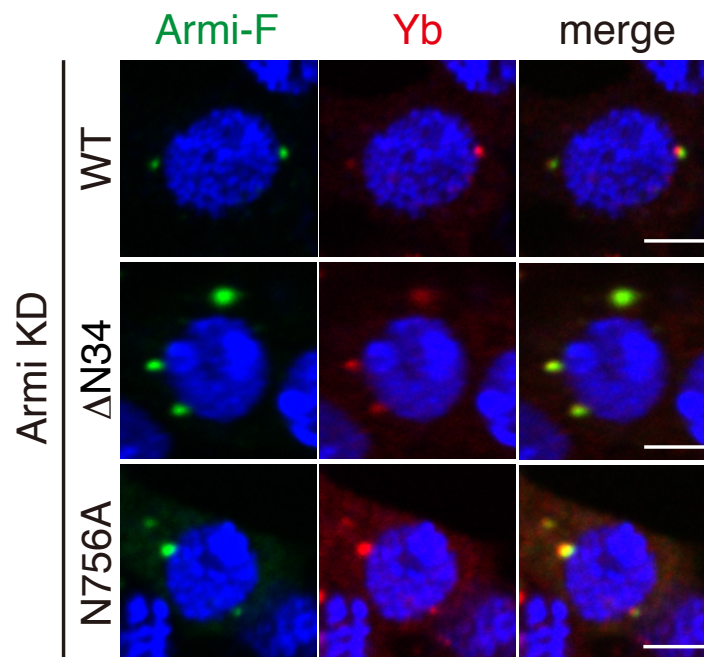


Figure 35. The behaviors of Armi mutants in Zuc-expressed cells. Armi-Flag (Armi-F) WT and Δ N34/N756A mutants (green) localized at Yb bodies (red) in Armi-depleted OSCs (Armi KD).

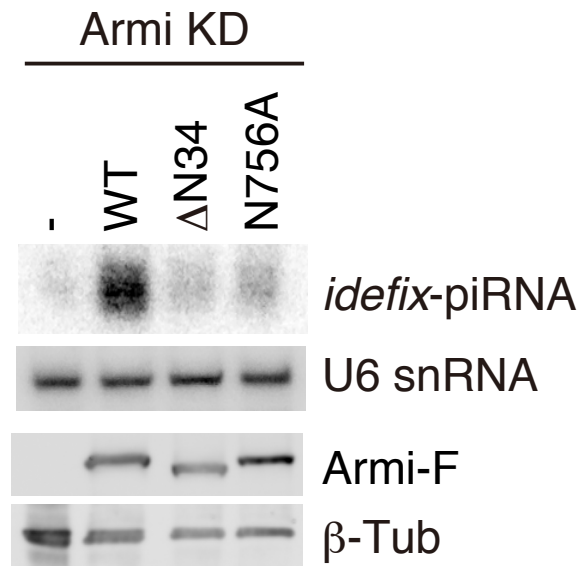


Figure 36. The RNA-binding activity and the N-terminus of Armi are indispensable for piRNA biogenesis.

Upper two lines: Northern blotting shows that siRNA-resistant WT Armi-Flag (Armi-F), but not Δ N34 and N756A mutants, rescued the defects in idfix-piRNA production caused by endogenous Armi depletion. U6 snRNA was used as a loading control. Lower two lines: The expression levels of Armi-Flag (Armi-F) WT, Δ N34, and N756A mutants. β -Tubulin was used as a loading control.

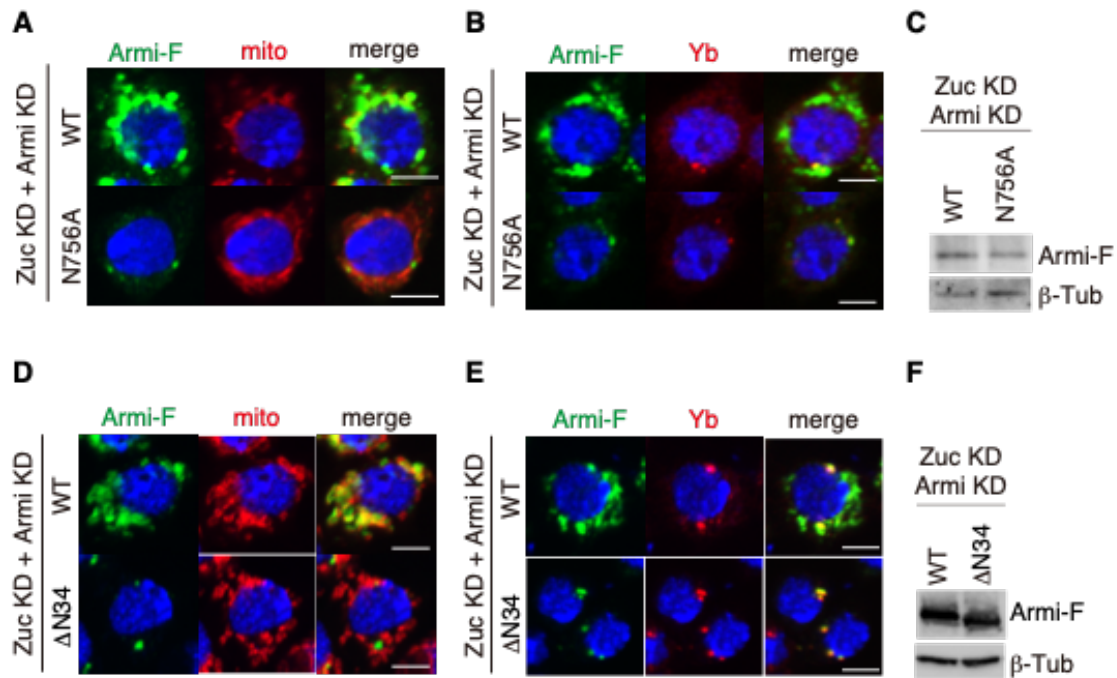


Figure 37. The RNA-binding activity and the N-terminus of Armi are required for the inter-organelle translocation

(A, D) Armi-Flag (Armi-F) WT and the N756A/ Δ N34 mutant were expressed in OSCs where endogenous Armi and Zuc had been depleted by RNAi (Zuc KD + Armi KD). Armi-F WT (green) localized onto mitochondria (red), whereas Armi-F N756A/ Δ N34 mutant (green) localized to Yb bodies. The scale bar represents 5 μ m. DAPI (blue) shows the nuclei. (B, E) Co-localization with Yb (red) is shown under the same condition of A and D. (C, F) The expression levels of Armi-Flag (Armi-F) WT and N756A/ Δ N34 mutant in Zuc/Armi-depleted OSCs (Zuc KD + Armi KD). β -Tubulin (β -Tub) was detected as a loading control.

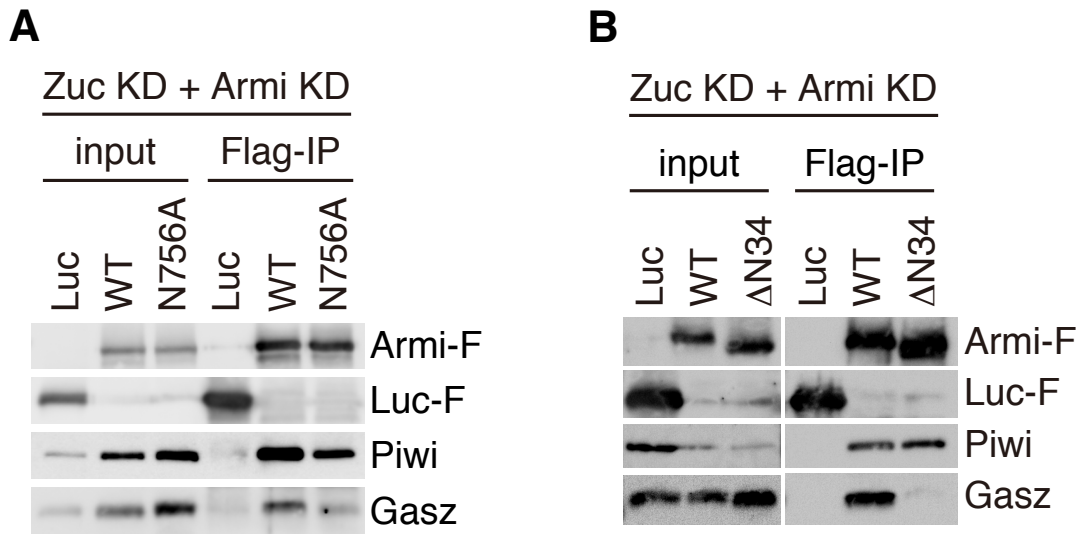


Figure 38. Both Δ N 34 and N756A mutants associated with Piwi but not with Gasz

(A, B) Armi-Flag (Armi-F) WT and the Δ N34/N756A mutant were expressed in OSCs where endogenous Armi and Zuc had been depleted by RNAi (Zuc KD + Armi KD). Immunoprecipitation and subsequent western blotting show that Armi-F WT but not Armi Δ N34/N756A mutant bound with Gasz in the cells. Both Armi WT and Δ N34/N756A mutant interacted with Piwi to similar extents. Luciferase-Flag (Luc-F) was used as a negative control.

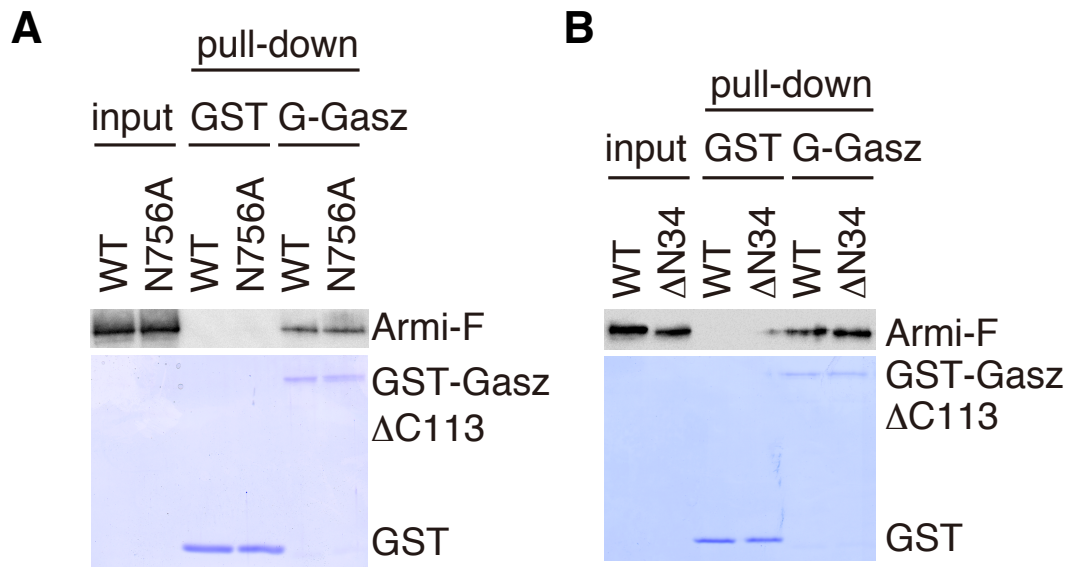


Figure 39. Both $\Delta N34$ and N756A mutants have direct interaction with Gasz

(A and B) In vitro pull-down assays show that both Armi-Flag (Armi-F) WT and $\Delta N34$ /N756A mutant directly bind with GST-Gasz $\Delta C113$ but not with GST. Armi-F WT and mutant were immunopurified from Schneider 2 (S2) cells under harsh conditions. GST and GST-Gasz $\Delta C113$ were visualized by CBB staining, while Armi-F WT and mutants were detected by western blotting using anti-Flag antibodies.

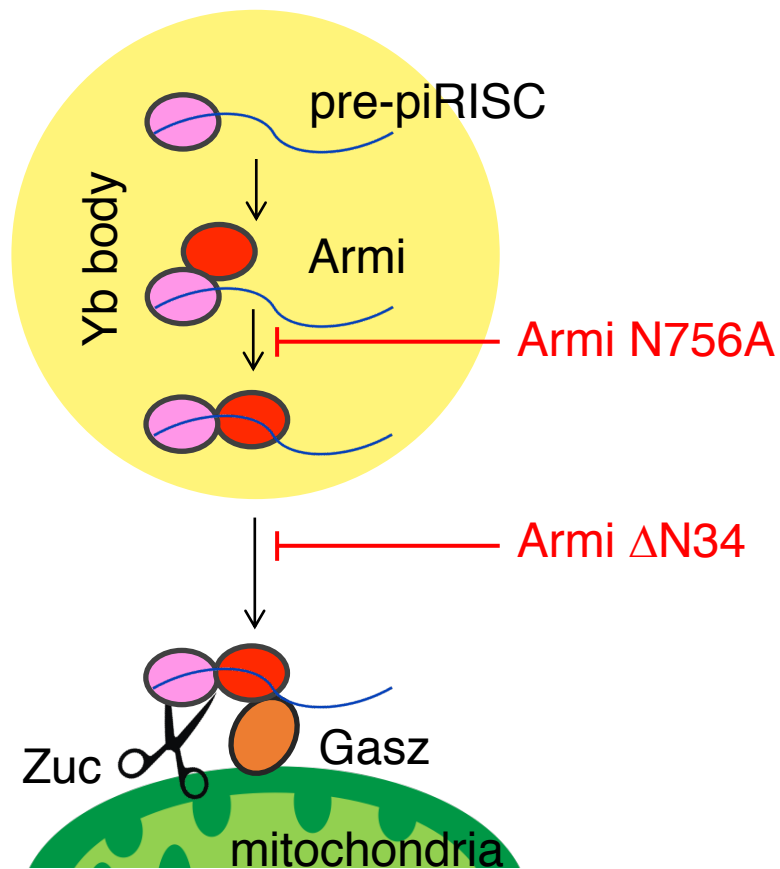


Figure 40. The behaviors of Armi mutants in OSCs

The Armi mutant N756A fails to bind piRNA precursors pre-bound with Piwi at Yb bodies, leading to the failure of pre-piRISC departure from Yb bodies. Another Armi mutant $\Delta N34$ is able to bind pre-piRISC at Yb bodies but fails to leave the bodies for an unknown reason.

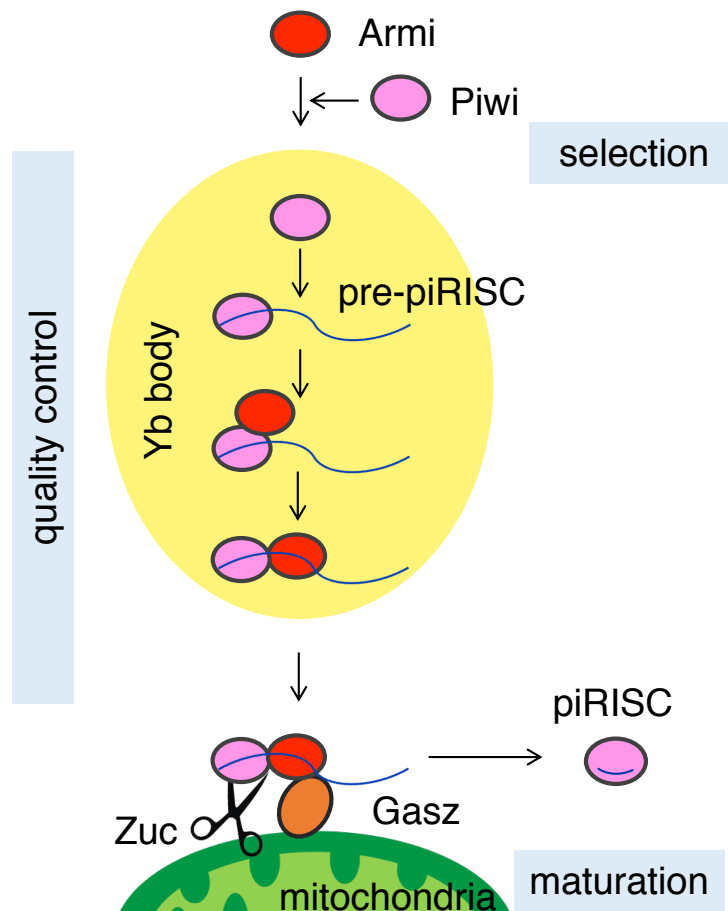


Figure 41. Proposed model for the molecular mechanism underlying the inter-organelle translocation of piRNA precursor

Armi localizes to Yb bodies Piwi-independently, but Piwi localization to Yb bodies depends on Armi. At Yb bodies, Piwi is loaded with piRNA precursor (through their 5' ends) to become pre-piRISC. Armi joins the complex by binding the downstream region in the precursor and also Piwi. The Armi-pre-piRISC complex then leaves Yb bodies to head to mitochondria for Zuc cleavage. The Armi-pre-piRISC complex is docked onto mitochondria through the Gasz complex, under which Zuc cleaves the precursor and releases piRISC to the cytosol. piRISC is translocated to the nucleus for transposon repression. The whole processing of piRISC-formation is well regulated by the interdependence between Armi and Piwi and also the RNA-binding activity of the two proteins in a multilayered manner.

Table

Table 1. Sequences of Oligonucleotides

siRNAs for RNAi in OSC

Name	sense	antisense
siZuc	GCAUUGCCGUCAGCACUGUTT	ACAGUGCUGACGGCAAUGCTT
siGasz	CGCUCGAAACCAGCUCCUUTT	AAGGAGCUGGUUUCGAGCGTT
siArmi	CAGCUUAAGGCGAAUCCAATT	UUGGAUUCGCCUUAAGCUGTT
siPiwi	GCUCCCAGGCGUGAAGGUGTT	CACCUUCACGCCUGGGAGCTT

primers for plasmid construction

Name	sequence	plasmid
pAcM-Gasz vectorF	AACAAGCTTGGTACCGAATTC	pAcM-Gasz
pAcM-Gasz vectorR	CAGGTCTTCTTCAGAGATCAGT	
pAcM-Gasz insertF	TCTGAAGAAGACCTGATGATGAGCAACCTTTGCAAA	pAcF-Gasz
pAcM-Gasz insertR	GGTACCAAGCTTGTCTATGAGAACCACCTTGCACTTG	
pAcF-Gasz vectorF	ATGATGAGCAACCTTTGCAAA	
pAcF-Gasz vectorR	CATGGTGGCTAGCCCG	
pAcF-Gasz insertF	GGGCTAGCCACCACATGGACTACAAAGACCATGACGG	pGEX-Gasz
pAcF-Gasz insertR	AAGGTTGCTCATCATCTTGTGCATCGTCATCCTTGTAATC	
pGEX-Gasz vectorF	CCGGAATTCCCGGGTC	
pGEX-Gasz vectorR	GGATCCCAGGGGCC	
pGEX-Gasz insertF	GGGCCCCCTGGGATCCATGATGAGCAACCTTTGCA	pGEX-GaszΔC133
pGEX-Gasz insertR	ACCCGGGAATTCGGCTATGAGAACCACCTTGCACTTG	
pGEX-GaszΔC133 inverseF	TAGCCGGAATTCCTCGG	
pGEX-GaszΔC133 inverseR	GATCTCATAGAAGTTGTTTCATCTCATC	
pAc-Armi-sires-F vectorF	CTCGAGGACTACAAAGACCAT	pAc-Armi-sires-F
pAc-Armi-sires-F vectorR	GGTGGCTAGCCCGAT	
pAc-Armi-sires-F insertF	ATCGGGCTAGCCACCACATGTTACATACGTTAGCAAGTT	pAc-ArmiN756A-sires-F
pAc-Armi-sires-F insertR	TTTGTAGTCCTCGAGGTTCAAATCATCTGTAGTATTCAGTGA	
pAc-ArmiN756A-sires-F inverseF	AGCTCAGCGGATTTGGTGAC	
pAc-ArmiN756A-sires-F inverseR	GGCCGACGGCGTTCCCAACAAGA	
pAc-ArmiΔN34-sires-F inverseF	ATGGAGGAGAAGATGGATCAG	pAc-ArmiΔN34-sires-F
pAc-ArmiΔN34-sires-F inverseR	GGTGGCTAGCCCGAT	
pAcF-PiwiPAZmt-sires vectorF	AGATCTATATCCAGCACAGTGG	pAcF-PiwiPAZmt-sires
pAcF-PiwiPAZmt-sires vectorR	AAGCTTGTCTTGTGCATCGTC	
pAcF-PiwiPAZmt-sires insertF	GACAAGAACAAGCTTGGTACCGAATTCTGCAGATATAAG	pAcF-PiwiMIDmt-sires
pAcF-PiwiPAZmt-sires insertR	GCTGGATATAGATCTTTATAGATAATAAACTTCTTTTCGAGCG	
pAcF-PiwiMIDmt-sires inverseF	GCCTCATCAATTAAGAGAGAGGATACGTT	
pAcF-PiwiMIDmt-sires inverseR	TCTTCGGCGTTATCATTGG	
pAc-Luc-F inverseF	ATCGGGCTAGCCACCACATGGAAGACGCCAAAAACATAAA	pAc-Luc-F
pAc-Luc-F inverseR	TTTGTAGTCCTCGAGCACGGCGATCTTCCGC	

probes for northern blotting

Name	sequence
ldefix-piRNA	AAACTACTGGCAATCGTTTGGGAA
U6 snRNA	GGGCCATGCTAATCTTCTCTCTGTA

References

References

Aravin AA, Naumova NM, Tulin AV, Vagin VV, Rozovsky YM, Gvozdev VA (2001) Double-stranded RNA-mediated silencing of genomic tandem repeats and transposable elements in the *D. melanogaster* germline. *Curr Biol* 11: 1017–1027

Brennecke J, Aravin AA, Stark A, Dus M, Kellis M, Sachidanandam R, Hannon GJ (2007) Discrete small RNA-generating loci as master regulators of transposon activity in *Drosophila*. *Cell* 128: 1089–1103

Carthew RW and Sontheimer EJ (2009) Origins and mechanisms of miRNAs and siRNAs. *Cell* 136: 642–655

Chakrabarti S, Jayachandran U, Bonneau F, Fiorini F, Basquin C, Domcke S, Le Hir H, Conti E (2011) Molecular mechanisms for the RNA-dependent ATPase activity of Upf1 and its regulation by Upf2. *Mol Cell* 41: 693–703

Cox DN, Chao A, Baker J, Chang L, Qiao D, Lin H (1998) A novel class of evolutionarily conserved genes defined by *piwi* are essential for stem cell self-renewal. *Genes Dev* 12: 3715–3727

Cox DN, Chao A, Lin H (2000) *piwi* encodes a nucleoplasmic factor whose activity modulates the number and division rate of germline stem cells. *Development* 127:503–514

Czech B, Munafò M, Ciabrelli F, Eastwood EL, Fabry MH, Kneuss E, Hannon GJ (2018) piRNA-guided genome defense: from biogenesis to silencing. *Annu Rev Genet* 52: 131–157

Czech B, Preall JB, McGinn J, Hannon GJ (2013) A transcriptome-wide RNAi screen in the *Drosophila* ovary reveals factors of the germline piRNA pathway. *Mol Cell* 50: 749–761

Davis-Dusenbery BN, Hata A (2010) Mechanisms of control of microRNA biogenesis. *J Biochem* 148: 381–392

Eulalio A, Huntzinger E, Izaurralde E (2008) GW182 interaction with Argonaute is essential for miRNA-mediated translational repression and mRNA decay. *Nat Struct Mol Biol* 15: 346–353

Fedoroff NV (2012) Transposable elements, epigenetics, and genome evolution. *Science* 338: 758–767

Feschotte C (2008) Transposable elements and the evolution of regulatory networks. *Nat Rev Genet* 9: 397–405

Fire A, Xu S, Montgomery MK, Kostas SA, Driver SE, Mello CC (1998) Potent and specific genetic interference by double-stranded RNA in *Caenorhabditis elegans*. *Nature* 391: 806–811

Gainetdinov I, Colpan C, Arif A, Cecchini K, Zamore PD (2018) A single mechanism of biogenesis, initiated and directed by PIWI proteins, explains piRNA production in most animals. *Mol Cell*: 71: 775-790

Ge DT, Wang W, Tipping C, Gainetdinov I, Weng Z, Zamore PD (2019) The RNA-binding ATPase, Armitage, couples piRNA amplification in nuage to phased piRNA production on mitochondria. *Mol Cell* 74: 982-995

Ghildiyal M, Zamore PD (2009) Small silencing RNAs: an expanding universe. *Nat Rev Genet* 10: 94–108

Goriaux C, Desset S, Renaud Y, Vaury C, Brassat E (2014) Transcriptional properties and splicing of the *flamenco* piRNA cluster. *EMBO Rep* 15: 411–418.

Gunawardane LS, Saito K, Nishida KM, Miyoshi K, Kawamura Y, Nagami T, Siomi H, Siomi MC (2007) A slicer-mediated

mechanism for repeat-associated siRNA 5' end formation in *Drosophila*. *Science* 315: 1587–1590

Ha M, Kim VN (2014) Regulation of microRNA biogenesis. *Nat Rev Mol Cell Biol* 15: 509–524

Han BW, Wang W, Li C, Weng Z, Zamore PD (2015) piRNA-guided transposon cleavage initiates Zucchini-dependent, phased piRNA production. *Science* 348: 817–821

Handler D, Meixner K, Pizka M, Lauss K, Schmied C, Gruber FS, Brennecke J (2013) The genetic makeup of the *Drosophila* piRNA pathway. *Mol Cell* 50: 762–777

Handler D, Olivieri D, Novatchkova M, Gruber FS, Meixner K, Mechtler K, Stark A, Sachidanandam R, Brennecke J (2011) A systematic analysis of *Drosophila* TUDOR domain-containing proteins identifies Vreteno and the Tdrd12 family as essential primary piRNA pathway factors. *EMBO J* 30: 3977–3993

Harris AN, Macdonald PM (2001) Aubergine encodes a *Drosophila* polar granule component required for pole cell formation and related to eIF2C. *Development* 128: 2823–2832.

Hirakata S, Ishizu H, Fujita A, Tomoe Y, Siomi MC (2019) Requirements for multivalent Yb body assembly in transposon silencing in *Drosophila*. *EMBO Rep* 20: e47708

Homolka D, Pandey RR, Goriaux C, Brassat E, Vaury C, Sachidanandam R, Fauvarque MO, Pillai RS (2015) PIWI slicing and RNA elements in precursors instruct directional primary piRNA biogenesis. *Cell Rep* 12: 418–428

Horwich MD, Li C, Matranga C, Vagin V, Farley G, Wang P, Zamore PD (2007) The *Drosophila* RNA methyltransferase DmHen1, modifies germline piRNAs and single-stranded siRNAs in RISC. *Curr Biol* 17: 1265–1272

Huang XA, Yin H, Sweeney S, Raha D, Snyder M, Lin H (2013) A major epigenetic programming mechanism guided by piRNAs. *Dev Cell* 24:502–516

Ipsaro JJ, Haase AD, Knott SR, Joshua-Tor L, Hannon GJ (2012) The structural biochemistry of Zucchini implicates it as a nuclease in piRNA biogenesis. *Nature* 491: 279–283

Ishizu H, Iwasaki YW, Hirakata S, Ozaki H, Iwasaki W, Siomi H, Siomi MC (2015) Somatic primary piRNA biogenesis driven by *cis*-

acting RNA elements and *trans*-acting Yb. *Cell Rep* 12: 429–440

Ishizu H, Kinoshita T, Hirakata S, Komatsuzaki C, Siomi MC (2019) Distinct and collaborative functions of Yb and Armitage in transposon-targeting piRNA biogenesis. *Cell Rep* 27: 1822–183

Ishizu H, Siomi H, Siomi MC (2012) Biology of PIWI-interacting RNAs: new insights into biogenesis and function inside and outside of germlines. *Genes Dev* 26: 2361–2373

Iwasaki S, Kawamata T, Tomari Y (2009) *Drosophila* Argonaute1 and Argonaute2 employ distinct mechanisms for translational expression. *Mol Cell* 34: 58–67

Iwasaki YW, Siomi MC, Siomi H (2015) PIWI-interacting RNA: its biogenesis and functions. *Annu Rev Biochem*: 405–433

Kazazian HH (2004) Mobile elements: drivers of genome evolution. *Science* 303: 1626–1632

Kim CA, Bowie JU (2003) SAM domains: uniform structure, diversity of function *Trends Biochem Sci* 28: 625–628

Kim VN, Han J, Siomi MC (2009) Biogenesis of small RNAs in animals. *Nat Rev Mol Cell Biol* 10: 126–139

Klattenhoff C, Theurkauf W (2008) Biogenesis and germline functions of piRNAs. *Development* 135: 3–9

Klenov MS, Sokolova OA, Yakushev EY, Stolyarenko AD, Mikhaleva EA (2011) Separation of stem cell maintenance and transposon silencing functions of Piwi protein. *PNAS* 108:18760–18765

Li J, Mahajan A, Tsai MD (2006) Ankyrin repeat: a unique motif mediating protein-protein interactions *Biochemistry* 45: 15168–15178

Li C, Vagin VV, Lee S, Xu J, Ma S, Xi H, Seitz H, Horwich MD, Syrzycka M, Honda BM, Kittler EL, Zapp ML, Klattenhoff C, Schulz N, Theurkauf WE, Weng Z, Zamore PD (2009) Collapse of germline piRNAs in the absence of Argonaute3 reveals somatic piRNAs in flies. *Cell* 137: 509–521

Lin H, Spradling AC (1997) A novel group of *pumilio* mutations affects the asymmetric division of germline stem cells in the *Drosophila* ovary. *Development* 124: 2463–2476

Ma L, Buchold GM, Greenbaum MP, Roy A, Burns KH, Zhu H, Han DY, Harris RA, Coarfa C, Gunaratne PH, Yan W, Matzuk MM (2009) *PLoS Genet* 5: e1000635

Malone CD, Brennecke J, Dus M, Stark A, McCombie WR, Sachidanandam R, Hannon GJ (2009) Specialized piRNA pathways act in germline and somatic tissues of the *Drosophila* ovary. *Cell* 137: 522–535

Matsumoto N, Nishimasu H, Sakakibara K, Nishida KM, Hirano T, Ishitani R, Siomi H, Siomi MC, Nureki O (2016) Crystal structure of silkworm PIWI-clade Argonaute Siwi bound to piRNA. *Cell* 167: 484–497

Miyoshi K, Tsukumo H, Nagami T, Siomi H, Siomi MC (2005) Slicer function of *Drosophila* Argonautes and its involvement in RISC formation. *Genes Dev* 19: 2837–2848

Mochizuki K, Fine NA, Fujisawa T, Gorovsky MA (2002) Analysis of a *piwi*-related gene implicates small RNAs in genome rearrangement in *tetrahymena*. *Cell* 110: 689–699

Mohn F, Handler D, Brennecke J (2015) piRNA-guided slicing

specifies transcripts for Zucchini-dependent, phased piRNA biogenesis. *Science* 348: 812–817

Mosavi LK, Cammett TJ, Desrosiers DC, Peng Z (2004) The ankyrin repeat as molecular architecture for protein recognition. *Protein Sci* 13: 1435–1448

Muerdter F, Guzzardo PM, Gillis J, Luo Y, Yu Y, Chen C, Fekete R, Hannon GJ (2013) A genome-wide RNAi screen draws a genetic framework for transposon control and primary piRNA biogenesis in *Drosophila*. *Mol Cell* 50: 736–748

Munafò M, Manelli V, Falconio FA, Sawle A, Kneuss E, Eastwood EL, Seah JWE, Czech B, Hannon GJ (2019) Daedalus and Gasz recruit Armitage to mitochondria, bringing piRNA precursors to the biogenesis machinery. *Genes Dev* 33: 844-856

Murota Y, Ishizu H, Nakagawa S, Iwasaki YW, Shibata S, Kamatani MK, Saito K, Okano H, Siomi H, Siomi MC (2014) Yb integrates piRNA intermediates and processing factors into perinuclear bodies to enhance piRISC assembly. *Cell Rep* 8: 103–113

Nguyen TN, Goodrich JA (2006) Protein-protein interaction

assays: eliminating false positive interactions. *Nat Methods* 3: 135–139

Nishida KM, Iwasaki YW, Murota Y, Nagao A, Mannen T, Kato Y, Siomi H, Siomi MC (2015) Respective functions of two distinct Siwi complexes assembled during PIWI-interacting RNA biogenesis in *Bombyx* germ cells. *Cell Rep* 10: 193–203

Nishimasu H, Ishizu H, Saito K, Fukuhara S, Kamatani MK, Bonnefond L, Matsumoto N, Nishizawa T, Nakanaga K, Aoki J, Ishitani R, Siomi H, Siomi MC, Nureki O (2012) Structure and function of Zucchini endoribonuclease in piRNA biogenesis. *Nature* 491: 284–287

Nye J, Buster DW, Rogers GC (2014) The use of cultured *Drosophila* cells for studying the microtubule cytoskeleton. *Methods Mol Biol* 1136: 81–101

Olivieri D, Senti KA, Subramanian S, Sachidanandam R, Brennecke J (2012) The cochaperone shutdown defines a group of biogenesis factors essential for all piRNA populations in *Drosophila*. *Mol Cell* 47: 954–969

Olivieri D, Sykora MM, Sachidanandam R, Mechtler K, Brennecke

J (2010) An *in vivo* RNAi assay identifies major genetic and cellular requirements for primary piRNA biogenesis in *Drosophila*. *EMBO J* 29: 3301–3317

Ozata DM, Gainetdinov I, Zoch A, O'Carroll D, Zamore PD (2019) PIWI-interacting RNAs: small RNAs with big functions. *Nat Rev Genet* 20: 89–108

Pandey RR, Homolka D, Chen KM, Sachidanandam R, Fauvarque MO, Pillai RS (2017) Recruitment of Armitage and Yb to a transcript triggers its phased processing into primary piRNAs in *Drosophila* ovaries. *PLoS Genet* 13: e1006956

Prud'homme N, Gans M, Masson M, Terzian C, Bucheton M (1995) *Flamenco*, a gene controlling the gypsy retrovirus of *Drosophila melanogaster*. *Genetics* 139: 697–711.

Saito K, Ishizuka A, Siomi H, Siomi MC (2005) Processing of pre-microRNAs by the Dicer-1-Loquacious complex in *Drosophila* cells. *PLoS Biol* 3: e235

Saito K, Inagaki S, Mituyama T, Kawamura Y, Ono Y, Sakota E, Kotani H, Asai K, Siomi H, Siomi MC (2009) A regulatory circuit for *piwi* by the large Maf gene *traffic jam* in

Drosophila. Nature 461: 1296–1299

Saito K, Ishizu H, Komai M, Kotani H, Kawamura Y, Nishida KM, Siomi H, Siomi MC (2010) Roles for the Yb body components Armitage and Yb in primary piRNA biogenesis in *Drosophila*. *Genes Dev* 24: 2493–2498

Saito K, Nishida KM, Mori T, Kawamura Y, Miyoshi K, Nagami T, Siomi H, Siomi MC (2006) Specific association of Piwi with rasiRNAs derived from retrotransposon and heterochromatic regions in the *Drosophila* genome. *Genes Dev* 20: 2214–2222

Saito, K, Sakaguchi Y, Suzuki T, Suzuki T, Siomi H, Siomi MC (2007) Pimet, the *Drosophila* homolog of HEN1, mediates 2'-O-methylation of Piwi-interacting RNAs at their 3' ends. *Genes Dev* 21: 1603–1608

Sato K and Siomi MC (2018) Two distinct transcriptional controls triggered by nuclear Piwi-piRISCs in the *Drosophila* piRNA pathway. *Curr Opin Struct Biol* 53: 69–76

Schupbach T, Wieschaus E (1991) Female sterile mutations on the second chromosome of *Drosophila Melanogaster*. II. mutations blocking oogenesis or altering egg morphology. *Genetics* 129: 1119–

1136.

Sienski G, Donertas D, Brennecke J (2012) Transcriptional silencing of transposons by Piwi and Maelstrom and its impact on chromatin state and gene expression. *Cell* 151:964–980

Siomi H, Siomi MC (2009) On the road to reading the RNA-interference code *Nature* 457: 396–404

Siomi MC, Sato K, Pezic D, Aravin AA (2011) PIWI-interacting small RNAs: The vanguard of genome defence. *Nat Rev Mol Cell Biol* 12: 246–258.

Slotkin RK and Martienssen R (2007) Transposable elements and the epigenetic regulation of the genome. *Nat Rev Genet* 8: 272–285

Szakmary A, Reedy M, Qi H, Lin H (2009) The Yb protein defines a novel organelle and regulates male germline stem cell self-renewal in *Drosophila melanogaster*. *J Cell Biol* 185: 613–627

Thomas LA, Rogers AK, Webster A, Marinov GK, Liao SE, Perkins EM, Hur JK, Aravin AA, Tóth KF (2013) Piwi induces piRNA-guided transcriptional silencing and establishment of a repressive

chromatin state. *Genes Dev* 27:390–399

Vagin VV, Sigova A, Li C, Seitz H, Gvozdev V, Zamore PD (2006) A distinct small RNA pathway silences selfish genetic elements in the germline. *Science* 313: 320–324

Vagin VV, Yu Y, Jankowska A, Luo Y, Wasik KA, Malone CD, Harrison E, Rosebrock A, Wakimoto BT, Fagegaltier D, Muerdter F, Hannon GJ (2013) Minotaur is critical for primary piRNA biogenesis. *RNA* 19: 1064–1077

Wang SH, Elgin SC. (2011) *Drosophila* Piwi functions downstream of piRNA production mediating a chromatin-based transposon silencing mechanism in female germ line. *PNAS* 108:21164–21169

Wieckowski MR, Giorgi C, Lebiedzinska M, Duszynski J, Pinton P (2009) Isolation of mitochondria-associated membranes and mitochondria from animal tissues and cells. *Nat Protoc* 4: 1582–1590

Wilson RC, Doudna JA. Molecular mechanisms of RNA interference. (2013) *Annu Rev Biophys* 42: 217–239.

Yamashiro H and Siomi MC (2018) PIWI-Interacting RNA in

Drosophila: biogenesis, transposon regulation, and beyond. *Chem Rev* 118: 4404–4421

Yashiro R, Murota Y, Nishida KM, Yamashiro H, Fujii K, Ogai A, Yamanaka S, Negishi L, Siomi H, Siomi MC (2018) Piwi nuclear localization and its regulatory mechanism in *Drosophila* ovarian somatic cells. *Cell Rep* 23: 3647–3657

Yu B, Yang Z, Li J, Minakhina S, Yang M, Padgett RW, Steward R, Chen X (2005) Methylation as a crucial step in plant microRNA biogenesis. *Science* 307: 932–935

Zamparini AL, Davis MY, Malone CD, Vieira E, Zavadil J, Sachidanandam R, Hannon GJ, Lehmann R (2011) Vreteno, a gonad-specific protein, is essential for germline development and primary piRNA biogenesis in *Drosophila*. *Development* 138: 4039–4050.

Zanni V, Eymery A, Coiffet M, Zytnicki M, Luyten I, Quesneville H, Vaury C, Jensen S (2013) Distribution, evolution, and diversity of retrotransposons at the *flamenco* locus reflect the regulatory properties of piRNA clusters *Proc Natl Acad Sci USA* 110: 19842–19847

Acknowledgements

Acknowledgements

First of all, I would like to express my deep and sincere gratitude to my supervisor, professor Dr. Mikiko C. Siomi for her stimulating suggestions, helps in writings, and a lot of precious opportunities as a Ph.D student in her laboratory. I am grateful to my mentor, Dr. Hirotsugu Ishizu for his considerable guidance and technical helps. I also appreciate to my colleagues, Mayu Negishi and Tatsuki Kinoshita for their help especially in the analyses of Piwi and Armi mutants. I thank Dr. Hitoshi Ohtani for his technical helps of anti-Gasz antibody production. I also thank the other members of Siomi laboratory for their discussions and comments on the manuscript. Finally, I would like to express my gratitude to my family for their warm encouragements and financial supports.

This work is supported by the Japan Society for the Promotion of Science.